Journal of Medicinal Chemistry

Article

pubs.acs.org/jmc

Phthalocyanine–Peptide Conjugates for Epidermal Growth Factor Receptor Targeting

Benson G. Ongarora,[†] Krystal R. Fontenot,[†] Xiaoke Hu,[†] Inder Sehgal,*[,‡] Seetharama D. Satyanarayana-Jois,[§] and dM. Graça H. Vicente*[,†]

[†]Louisiana State University, Department of Chemistry, Baton Rouge Louisiana 70803, United States

[‡]Louisiana State University, School of Veterinary Medicine, Baton Rouge Louisiana 70803, United States

[§]University of Louisiana at Monroe, College of Pharmacy, Monroe Louisiana 71201, United States

Supporting Information

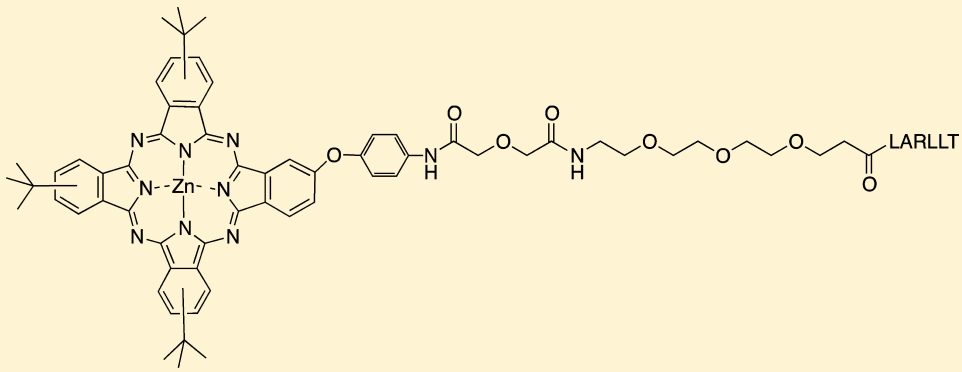

ABSTRACT: Four phthalocyanine (*Pc*)–peptide conjugates designed to target the epidermal growth factor receptor (EGFR) were synthesized and evaluated in vitro using four cell lines: human carcinoma A431 and HEp2, human colorectal HT-29, and kidney Vero (negative control) cells. Two peptide ligands for EGFR were investigated: EGFR-L1 and -L2, bearing 6 and 13 amino acid residues, respectively. The peptides and *Pc*-conjugates were shown to bind to EGFR using both theoretical (Autodock) and experimental (SPR) investigations. The *Pc*–EGFR-L1 conjugates **5a** and **5b** efficiently targeted EGFR and were internalized, in part due to their cationic charge, whereas the uncharged *Pc*–EGFR-L2 conjugates **4b** and **6a** poorly targeted EGFR maybe due to their low aqueous solubility. All conjugates were nontoxic (IC_{50} > 100 μM) to HT-29 cells, both in the dark and upon light activation (1 J/cm^2). Intravenous (iv) administration of conjugate **5b** into nude mice bearing A431 and HT-29 human tumor xenografts resulted in a near-IR fluorescence signal at ca. 700 nm, 24 h after administration. Our studies show that *Pc*–EGFR-L1 conjugates are promising near-IR fluorescent contrast agents for CRC and potentially other EGFR overexpressing cancers.

INTRODUCTION

Colorectal cancer (CRC) is currently the second leading cause of cancer-related deaths among both men and women in the US.[1] Colon cancer typically develops over several years and in a linear fashion from adenomatous polyps to carcinoma. Routine colon screening, detection, and removal of polyp adenomas and early stage cancer reduces the incidence of CRC; however, because the disease lacks outward signs or symptoms, most cancers are detected at a stage where they may become terminal.[2] Current methods of detection for CRC include flexible sigmoidoscopy, standard colonoscopy, radiography, and computer tomography (CT) colonoscopy, which identify large adenoma lesions but frequently miss small adenomas (<5 mm) and flat lesions, two early stages of CRC.[2] Improvements in the early detection of small adenomas and flat lesions could prevent the development of malignant tumors, decreasing mortality and overall health care cost. New detection methods currently being employed to accomplish this goal include chromoendoscopy, narrow band imaging, and blue light autofluorescence.[3] Chromoendoscopy utilizes an absorptive or contrast dye, such as methylene blue, to stain the mucosa for standard white light colonoscopy, enhancing tissue characterization, differentiation, and diagnosis of small adenomas.[2,3] Narrow band imaging uses a blue and green filter to narrow the white colonoscopic light to illuminate the mucosa, and blue light autofluorescence involves a UV light source to generate mucosal autofluorescence. In addition, confocal laser endomicroscopy (CLE) has been employed to image the mucosa, with fluorescein, acriflavine, or cresyl violet as the fluorescent dyes. Drawbacks of these dyes are their poor selectivity for CRC, residual toxicity, and emission wavelengths in the visible region of the optical spectrum.[4] On the other hand, phthalocyanines (*Pcs*) are tetrapyrrolic macrocycles with extended π-conjugated

Received: November 15, 2011
Published: April 2, 2012

Scheme 1[a]

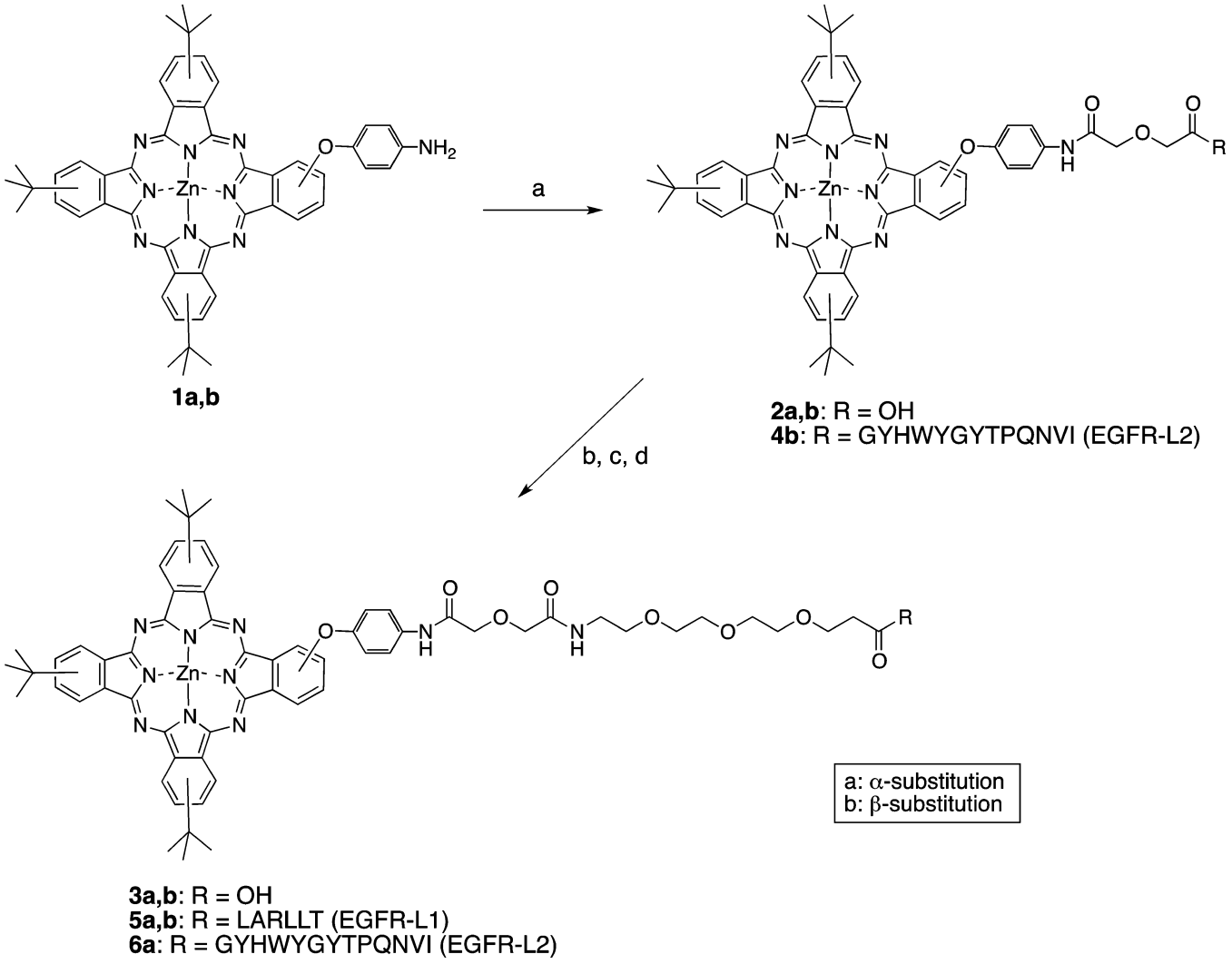

[a]Conditions: (a) 1,4-dioxane-2, 6-dione, DMF, rt, (87−92%); (b) *tert*-butyl-12-amino-4,7,10-trioxadodecanoate, DIEA, HOBt, EDCI, DMF, 72 h, rt, (77−82%); (c) TFA, dichloromethane, 4 h, (88−89%); (d) DIEA, HOBt, TBTU, EGFR-L1 or EGFR-L2, DMF, 24 h, then TFA/H_2O/phenol/TIS 88/5/5/2 (20−80%).

systems that typically emit at long wavelengths (>670 nm) with relatively high fluorescence quantum yields.[5,6] Advantages of near-IR fluorescence for bioimaging applications include low Raman scattering cross sections associated with the use of low energy excitation photons, larger Raman-free observation windows, and reduced absorption and fluorescence from other compounds.[7] *Pcs* have been extensively investigated in the last decades for a variety of applications, including as colorant dyes, catalysts, sensors, and as photosensitizers for photodynamic therapy (PDT) of cancers.[8−10] PDT involves the administration of a photosensitizer followed by activation with red light to produce cytotoxic oxygen species that destroy malignant cells.[11,12] Because of their low dark toxicity, high photostability, and ability for preferential accumulation within tumor tissue, *Pcs* are promising cancer diagnostic and treatment agents. Furthermore, conjugation of *Pcs* with peptide ligands directed at specific receptors overexpressed in cancer cells, such as the human epidermal growth factor receptor (EGFR), is an attractive strategy for increasing their biological efficacy.[13−17] EGFR is overexpressed in CRC, including small cancers (<5 mm) and the flat, dysplastic, aberrant crypt foci that are believed to precede cancer development.[18−20] Among the EGFR-targeting biomolecules recently reported for selective delivery of cytotoxic drugs to the tumor sites,[21−25] two small peptides with sequences LARLLT (designated EGFR-L1)[26] and YHWYGYTPQNVI (designated EGFR-L2)[27] are particularly attractive due to their readily availability, low immunogenicity, ease of conjugation to various molecules, and reported superior EGFR-targeting ability. EGFR-L1 was selected from computational screening of an EGFR peptide ligand virtual library and shown to target EGFR both in vitro (in EGFR overexpressing H1299 cells) and in vivo (in H1299 tumor-bearing mice following intravenous (iv) administration).[26] On the other hand, EGFR-L2 was identified from screening of a phage display peptide library and also shown to bind to EGFR both in vitro (SMMC-7721 cells) and in vivo (SMMC-7721 tumor bearing mice following iv injection).[27] In our continuing investigation of tumor-selective fluorescent imaging and PDT agents, we have recently shown that a *Pc* conjugated to a bifunctional nuclear localizing sequence and cell penetrating peptide containing 32 amino acid residues, via either a short (5-atom) or a PEG (20-atom) linker, displays

dx.doi.org/10.1021/jm201544y | J. Med. Chem. 2012, 55, 3725−3738

higher fluorescence quantum yield and increased cellular uptake compared with unconjugated *Pc*.[28] We now report the synthesis, photophysical, and biological evaluation of *Pc* conjugates to either EGFR-L1 or EGFR-L2 peptide ligands.

RESULTS AND DISCUSSION

1. Synthesis and Characterization. The *Pc*–peptide conjugates described in this study were designed to specifically target EGFR. The synthetic route to conjugates **4b**, **5a**, **5b**, and **6a** is shown in Scheme 1. *Pcs* **1a**,**b** were prepared by statistical condensation of 3- or 4-(*p*-*N*-Boc-aminophenoxy)phthalonitrile and 4-*tert*-butylphthalonitrile (in 1:3 ratio) in DMAE at 140 °C for 5 h, and in the presence of Zn(II) acetate and DBN, followed by TFA cleavage of the Boc groups, as we have previously described.[29] Reaction of *Pcs* **1a**,**b** with diglycolic anhydride in DMF gave the corresponding α- or β-substituted carboxy-terminated Pcs **2a**,**b**, respectively, in 87–92% yields.[28,38] The coupling of Pcs **2a**,**b** with commercially available *tert*-butyl protected PEG using HOBt, EDCI, and DIEA, following by deprotection of the *tert*-butyl group, afforded the *Pcs* **3a**,**b** in 68–73% overall yields;[38] lower yields were obtained when TBTU was used in place of EDCI due to a more difficult purification of the target *Pc*–PEG compounds. Solid-phase conjugation of *Pcs* **2b**, **3a**, and **3b** to the two peptide sequences LARLLT[26] (EGFR-L1) and GYHWYGYTPQNVI[27] (EGFR-L2) using DIEA, HOBt, and TBTU or HATU in DMF and at room temperature gave the targeted *Pc*–peptide conjugates **4b**, **5a**, **5b**, and **6a** in 20–80% yields, after deprotection and cleavage from the solid support, followed by reversed-phase chromatographic purification. A glycine residue was added to the N-terminus of the EGFR-L2 peptide in order to increase the conjugation reaction yields.[38,39]

EGFR overexpression has been found in a variety of human cancers, including breast, ovarian, prostate, pancreatic, and colorectal;[40] for this reason EGFR has been an important target for cancer treatment.[13−17] Monoclonal antibodies (mAbs), such as cetuximab and trastuzumab, and tyrosine kinase inhibitors (TKIs), such as erlotinib and gefitinib, are HER1/EGFR-targeted agents currently in clinical development, or already approved, for use in several countries. Peptides EGFR-L1 and EGFR-L2 were designed to act as a substitute for the natural ligand EGF, which has been reported to have mitogenic and neoangiogenic activity and has been shown to specifically target EGFR overexpressing tumor cells both in vitro and in vivo.[26,27] Advantages of using small peptide ligands as target units are their easy synthesis and coupling to fluorophores and their low immunogenicity and high binding affinity for the biological target. We have previously conjugated a *Pc* macrocycle to a lysine-rich bifunctional peptide sequence containing 32 amino acid residues, via a similar short (5-atom) and a long (20-atom) PEG linker, and observed that the PEG linker increased cellular uptake into human HEp2 cells and decreased cytotoxicity of the *Pc* conjugate.[28] On the other hand, the short linker *Pc* conjugate showed higher fluorescence quantum yield, probably as a result of its lower conformational flexibility compared with the PEG group. In the present study, we investigated a short (5-atom) and a low-molecular-weight PEG (13-atom) linkers between the *Pc* and the peptide ligand; the smaller PEG group has the advantages of being commercially available and potentially less flexible than the penta(ethylene glycol) previously used. In addition, the PEG linker is believed to favor an extended conformation for conjugates **5a**,**b** and **6a**,[38] which might favor EGFR target binding and to increase their aqueous solubility compared with conjugate **4b** (vide infra).

All Pcs were characterized by MS, NMR, UV–vis, and fluorescence spectroscopy; MALDI-TOF was used to confirm the amino acid sequence in the *Pc*–peptide conjugates (see Supporting Information, Figures S22–S52). The spectroscopic properties for *Pcs* **3a**,**b**, **4b**, **5a**,**b** and **6a** are summarized in Table 1 and Figure S18 of the Supporting Information). All *Pcs* showed strong Q absorption bands between 677–680 nm in DMF and emissions between 680–683 nm in the same solvent, with fluorescence quantum yields in the range 0.10–0.13 and Stokes' shifts of 2–4 nm, characteristic of this type of compound.[28,29] All *Pc*–peptide conjugates are soluble in polar organic solvents, such as DMSO and DMF, up to 1.0 mM concentrations, however precipitation was observed upon dilution into aqueous solutions. Therefore, Cremophor EL, a nonionic solubilizer and emulsifier, was added to all *Pc* stock solutions used in the biological and EGFR-binding experiments; the cell studies were conducted in PBS/DMSO/Cremophor (94:1:5) and the mice studies in PBS/DMSO/Cremophor (85:10:5). No toxic effects were observed in vitro nor in vivo from these amounts of DMSO and Cremophor EL (see Figure S57 of the Supporting Information).

Table 1. Spectroscopic Properties of *Pcs* in DMF

Pc	absorption (nm)	emission[a] (nm)	Stokes' shift	ε (M^{-1} cm^{-1})[1]	Φ_F[b]
3a	678	682	4	5.35	0.10
3b	677	680	3	5.19	0.13
4b	677	681	4	4.85	0.10
5a	680	683	3	5.33	0.12
5b	680	682	2	5.27	0.11
6a	680	683	3	4.60	0.13

[a]Excitation at 670 nm. [b]Calculated using ZnPc (Φ_f = 0.17) as the standard.

The solubility of the *Pcs* decreased in the order *Pc*–PEG (**3a**,**b**) > *Pc*–EGFR-L1 (**5a**,**b**) > *Pc*–EGFR-L2 (**6a**) > *Pc*–EGFR-L2 (**4b**) due to the high hydrophobicity of the longer EGFR-L2 sequence (containing 11 hydrophobic amino acids and only two polar), compared with EGFR-L1 (containing 4 hydrophobic amino acids, one polar and one cationic). Indeed, the uncharged *Pc* conjugates **4b** and **6a** showed decreased solubility in polar protic solvents such as methanol compared with the positively charged *Pc* conjugates **5a**,**b**. The least soluble was the *Pc*–EGFR-L2 conjugate **4b** bearing a short 5-atom linker.

2. Docking and Binding Studies. To model the interaction of peptides EGFR-L1 and EGFR-L2 and their *Pc* conjugates with EGFR, docking studies were carried out using Autodock.[32,33] EGFR-L1 is known to bind to a pocket away from the EGF binding pocket in EGFR,[26] while EGFR-L2 binds to the EGF binding pocket.[27] Hence, for EGFR-L1 the grid box for docking calculations was around Glu71, Asn134, and Gly177. The low-energy docked structure (docking energy of −6.06 kcal/mol) of EGFR-L1 is shown in Figure 1a. The Leu4 backbone carbonyl and Thr6 side chain hydroxyl groups form hydrogen-bonding interaction with EGFR. The RLLT sequence of the peptide acquired a β-turn conformation when bound to the receptor EGFR.

The low-energy docked structure of EGFR-L2 peptide is shown in Figure 1b. EGFR-L2 peptide binds to the EGF

dx.doi.org/10.1021/jm201544y | J. Med. Chem. 2012, 55, 3725–3738

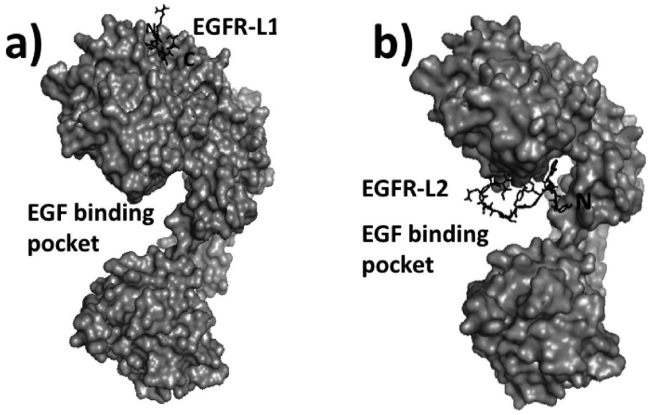

Figure 1. Low-energy docked structure of (a) EGFR-L1 and (b) EGFR-L2 peptides with EGFR receptor. EGFR is shown in surface, and the peptide is shown as dark sticks. The EGF binding pocket is shown.

binding pocket with docking energy of −5.96 kcal/mol. Tyr2 and Ile13 residues from the peptide formed hydrogen-bonding interactions with the EGFR stabilizing the peptide−receptor interaction. Overall, the peptide did not have any particular secondary structure as shown in Figure 1b. Peptide was bound in the cavity of EGF binding pocket of EGFR. These results indicate that both peptides EGFR-L1 and EGFR-L2 can bind to EGFR.

To evaluate the effect of conjugation on binding to EGFR and the linker size, docking studies were performed on *Pc* conjugates **4b**, **5b**, and **6a**. In *Pc*−EGFR-L2 **4b**, the peptide is conjugated via a short (5-atom) linker, in **6a** via a 13-atom PEG linker, while in *Pc*−EGFR-L1 **5b** the peptide is conjugated via a 13-atom PEG linker. Docking of **4b** and **6a** were similar to that of EGFR-L2 (see Figure S55 of the Supporting Information). However, the docking energies obtained for conjugates **4b** and **6a** were lower (with a docking intermolecular energy of −17 kcal/mol for **4b** and −8 kcal/mol for **6a**) than that of peptide EGFR-L2 alone (−6 kcal/mol). Conjugates **4b** and **6a** were docked to the EGF binding site, with the *Pc* macrocycle extending outside the EGF binding pocket and anchoring near the hydrophobic region around amino acid residues Tyr89, Tyr93, and Phe148 of EGFR. On the other hand, *Pc*−EGFR-L1 conjugate **5b** showed lower docking energy (−12 kcal/mol) compared with the peptide alone (−6 kcal/mol). The peptide part of **5b** was bound to a groove near amino acids Lys56, Asn79, Glu181, and Lys185 of EGFR, which are away from the binding site of EGF. The *Pc* part of conjugate **5b** was anchored to the other face around Pro171 of EGFR (see Figure S56 of the Supporting Information). These results suggest that the *Pc*−peptide conjugates should bind to EGFR with even higher affinity than the peptides alone. A surface plasmon resonance (SPR) binding assay[36,37] was performed to confirm binding of the peptides and *Pc* conjugates **5b** and **6a** to EGFR (see Table S1 and Figure S58 of the Supporting Information). EGFR was immobilized on the chip surface, and the relative binding of different ligands was analyzed. The binding of high affinity ligand EGF to EGFR was clearly seen in SPR. Other ligands and *Pc* conjugates reported in this study showed relatively lower affinity to EGFR. Conjugate **6a** was found to have the highest affinity for EGFR, followed by **5b**. The peptides alone bound with lower affinities than the *Pc* conjugates, and EGFR-L2 showed higher affinity for EGFR than EGFR-L1, in agreement with the docking studies. The *Pc*−PEG **3b** was also observed to bind to EGFR but with lower affinity than the *Pc*−peptide conjugates.

3. Cell Culture. Four cell lines with different EGFR expressions were used to investigate the cytotoxicity, uptake, and subcellular distribution of *Pc*−peptide conjugates **4b**, **5a**, **5b**, and **6a**: human squamous cell carcinoma HEp2,[28,29,38,39] human epidermoid carcinoma A431,[41−43] *Cercopithecus aethiops* kidney Vero (as negative control),[44] and human colorectal adenocarcinoma HT-29 cells.[45−47] The model human HEp2 cells are often used in the investigation of peptide−fluorophore conjugates, while the human A431 cells are a positive control for high EGFR expression (∼1−3 million EGFR per cell) and the African green monkey Vero cells are a negative control (lowest expression of EGFR). The human colorectal adenocarcinoma HT-29 cells overexpress EGFR, although to a lower degree (∼9000 EGFR per cell) than the A431 cells.[45−47]

3.1. Cytotoxicity. The dark- and photocytotoxicity for *Pc*−PEG **3a** and *Pc*−peptide conjugates **4b**, **5a**,**b**, and **6a** were evaluated in all cell lines at concentrations up to 125 μM, using the Cell Titer Blue Assay, and the results are summarized in Table 2 and shown in Figures S20 and S21 of the Supporting Information. None of the *Pcs* was found to be toxic in the dark, with determined IC_{50} values for all *Pcs* above 125 μM, the highest concentration investigated. Upon exposure to a low light dose (1 J/cm^2), only *Pc* **5a** bearing the EGFR-L1 peptide was found toxic to A431, HEp2, and Vero cells (IC_{50} = 16, 17, and 47 μM, respectively). In human carcinoma HEp2 cells, *Pc* conjugate **5a** was significantly more phototoxic than **5b** (IC_{50} ∼ 100 μM), in agreement with our recent observations showing that α-substituted *Pcs* tend to be more phototoxic than the corresponding β-substituted *Pcs*.[29] On the other hand, none of the Pcs were phototoxic to human HT-29 cells, suggesting that this type of conjugate could potentially be used for imaging of colorectal tumors. Low toxicity is an important feature of potential new imaging agents to be employed in conjunction with CLE. The *Pc*−EGFR-L1 conjugate **5a** was significantly more phototoxic than the corresponding *Pc*−EGFR-L2 conjugate **6a**, which might be a result of its higher uptake into cells due to its cationic charge (vide infra). The presence of the PEG linker did not have an effect on the observed cytotoxicity of the conjugates although it increased their aqueous solubility.

Table 2. Dark and Photo Cytotoxicity for *Pc* Conjugates Using the Cell Titer Blue Assay

compd	A431 cells IC_{50} (μM) light/dark	Vero cells IC_{50} (μM) light/dark	HEp2 cells IC_{50} (μM) light/dark	HT-29 cells IC_{50} (μM) light/dark
3a	>100/>125	>100/>125	>100/>125	>100/>125
4b	>100/>125	>100/>125	>100/>125	>100/>125
5a	15.8/>125	47.0/>125	17.0/>125	>100/>125
5b	>100/>125	>100/>125	>100/>125	>100/>125
6a	>100/>125	>100/>125	>100/>125	>100/>125

3.2. Time-Dependent Uptake. The time-dependent cellular uptake for all *Pcs* was performed at the nontoxic concentration of 10 μM in all cell lines, and the results are shown in Figure 2. There were marked differences in the cellular uptake of the *Pc*−EGFR-L1 conjugates compared with the *Pc*−EGFR-L2 conjugates, which might be due to their different overall charge, solubility, and tendency for aggregation. While the

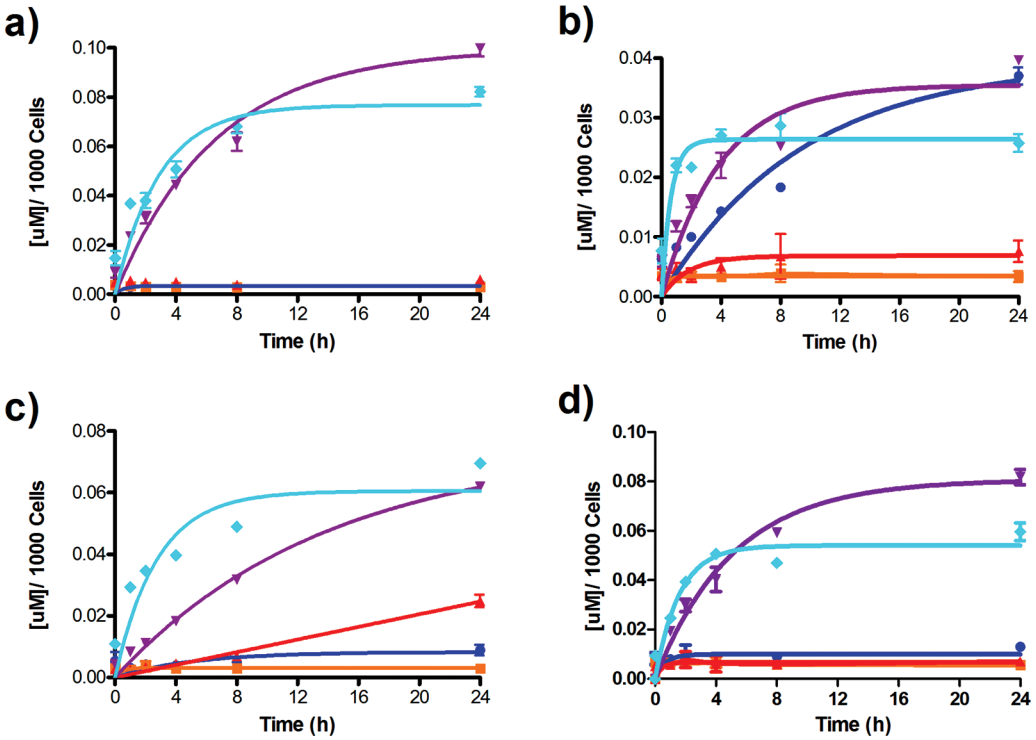

Figure 2. Time-dependent uptake of Pcs **3a** (blue), **4b** (orange), **5a** (purple), **5b** (turquoise), and **6a** (red) at 10 μM by (a) A431, (b) Vero, (c) HEp2, and (d) HT-29 cells.

highly hydrophobic and uncharged *Pc*–EGFR-L2 conjugates **4b** and **6a** were poorly taken up by all cell lines, in particular by A431 and HT-29 cells which overexpress EGFR, the positively charged *Pc*–EGFR-L1 conjugates **5a** and **5b** accumulated within cells to a much higher extent. Cells with higher EGFR expression showed higher uptake of the *Pc* conjugates, about 4-fold increase in A431 vs Vero cells, and a 3- or 2-fold increase in HT-29 colorectal and HEp2 cancer cells, respectively. This result shows that *Pc* conjugates **5a** and **5b** can indeed target cancer cells overexpressing EGFR, in particular CRC cells. It is interesting to compare the very different *Pc* uptake into Vero cells, with low expression of EGFR; *Pc* conjugate **5b** accumulated the fastest, followed by **5a** and precursor *Pc*–PEG **3a**. The *Pc*–EGFR-L2 conjugates **4b** and **6a** were taken up by Vero cells to a much lower extent than the *Pc*–EGFR-L1 conjugates **5a**,**b** and **6a** bearing a PEG linker accumulated ∼2-fold higher than **4b**. These results show that the *Pc* macrocycle has a natural tendency to accumulate within cells, with or without overexpression of EGFR, and that the PEG-containing compounds tend to be taken up to a higher extent. The conjugation of the *Pc* to a small cationic peptide sequence (EGFR-L1) changes the uptake kinetics, as seen in Figure 2b, and as previously observed.[39] In EGFR overexpressing cells, *Pc* conjugates **5a** and **5b** clearly were taken up the most of all Pcs investigated. For example, in A431 cells, conjugates **5a** and **5b** accumulated ∼15-fold more than *Pc*–PEG **3a** and than the *Pc*–EGFR-L2 conjugates **4b** and **6a** (Figure 2a). Similarly, in HT-29 and HEp2 cells, **5a** and **5b** were taken up to a significant higher extent than Pcs **3a**, **4b**, and **6a**. These results indicate that the peptide sequence has a marked effect on the cell targeting and uptake ability of the *Pc* conjugates. Autodock and SPR investigations show that peptides EGFR-L1 and EGFR-L2, and *Pc* conjugates **4b**, **5b**, and **6a** bind to EGFR (vide supra). Although *Pc*–EGFR-L2 conjugates can bind to EGFR with high specificity and be retained at the cell surface rather than internalized, their low uptake into Vero cells with low expression of EGFR suggests that their low solubility and high tendency for aggregation are responsible for their observed low cellular uptake. Indeed, the least soluble *Pc* **4b** accumulated the least within cells compared with all *Pcs* investigated, although this conjugate gave the lowest docking energy (−17 kcal/mol) of all molecules investigated. On the other hand, the *Pc*–EGFR-L1 conjugates bearing an arginine residue and overall +1 charge were readily taken up by all cells, as we have previously observed for porphyrin–peptide conjugates bearing 1–4 positively charged residues.[48] Positively charged molecules have been observed to have enhanced ability for crossing negatively charged plasma membranes, in particular those containing arginine due to the unique ability of the protonated guanidinium group to form bidentate hydrogen bonds.[48−52]

Of all *Pc*–peptide conjugates investigated, **5b** accumulated the fastest within all cell lines, followed by **5a**, which was found in the highest amount within A431 and HT-29 cells, at times >8 h after *Pc* exposure. Because of its rapid and efficient uptake into cells and low cytotoxicity, *Pc* conjugate **5b** was chosen for further investigation in animal studies (vide infra).

3.3. Subcellular Localization. The preferential sites of intracellular localization of *Pc*–peptide conjugates **4b**, **5a**,**b**, and **6a** and *Pc*–PEG **3a** were evaluated using fluorescence microscopy in the three human cell lines overexpressing EGFR, i.e., A431, HT-29, and HEp2 cells. The results are summarized in Table 3 and shown in Figures 3 and 4 for conjugate **5b** and in the Supporting Information, Figures S1–S13. Co-localization experiments were performed using the organelle-specific probes LysoTracker Green (lysosomes), ER Tracker Blue/White (ER), MitoTracker Green (mitochondria), and BODIPY Ceramide (Golgi). All conjugates localized in

dx.doi.org/10.1021/jm201544y | J. Med. Chem. 2012, 55, 3725–3738

Table 3. Main Subcellular Sites of Localization for Pc Conjugates in Human Cells

compd	A431 cells	HEp2 cells	HT-29 cells
3a	Lyso, Golgi, Mito	Lyso, Golgi	Lyso
4b	Lyso, Golgi, Mito	Lyso, Golgi, Mito	Lyso, Golgi, Mito
5a	Lyso, Golgi, Mito, ER	Lyso, Golgi, Mito, ER	Lyso, Mito
5b	Lyso, Golgi, Mito	Lyso, Golgi, Mito	Lyso, Golgi, Mito
6a	Lyso, Golgi, Mito	Lyso, Golgi, Mito	Lyso, ER

multiple sites within the cells. The *Pc*–EGFR-L1 conjugate **5b** was found in the lysosomes, mitochondria, and Golgi of all cell lines; in addition, its regioisomer **5a** was also observed in the ER, which might in part explain its higher phototoxicity

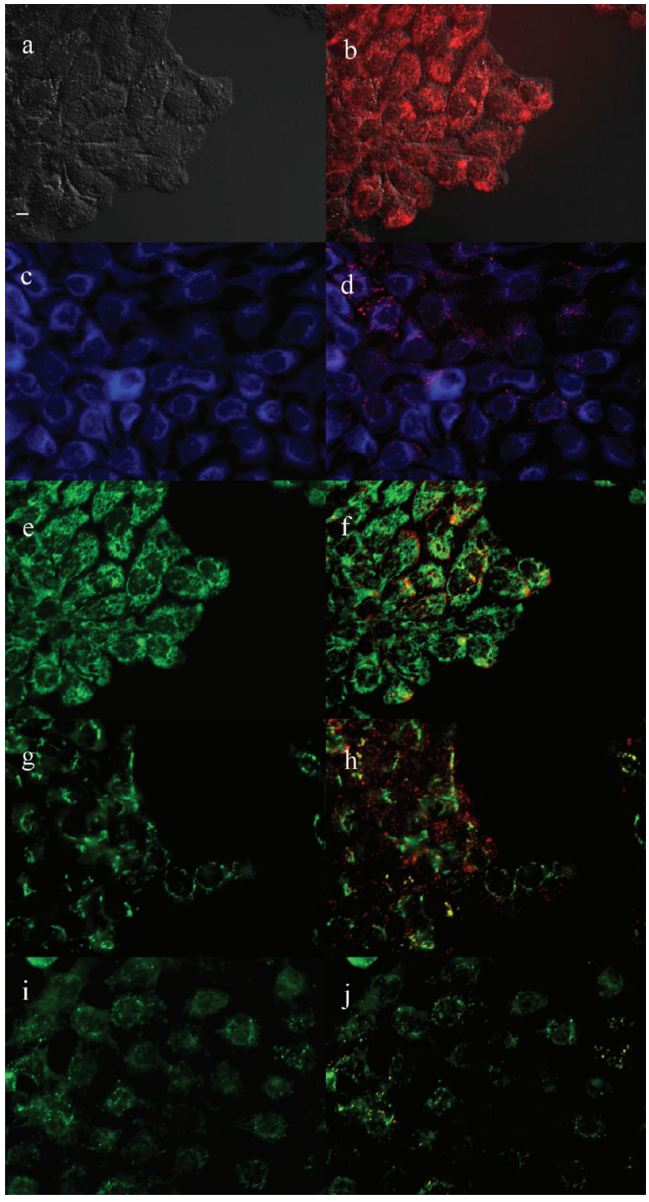

Figure 3. Subcellular fluorescence of *Pc* **5b** in A431 cells at 10 μM for 6 h. (a) Phase contrast, (b) overlay of **5b** fluorescence and phase contrast, (c) ER Tracker Blue/White fluorescence, (e) MitoTracker Green fluorescence, (g) BODIPY Ceramide, (i) LysoSensor Green fluorescence, and (d, f, h, j) overlays of organelle tracers with **5b** fluorescence. Scale bar: 10 μm.

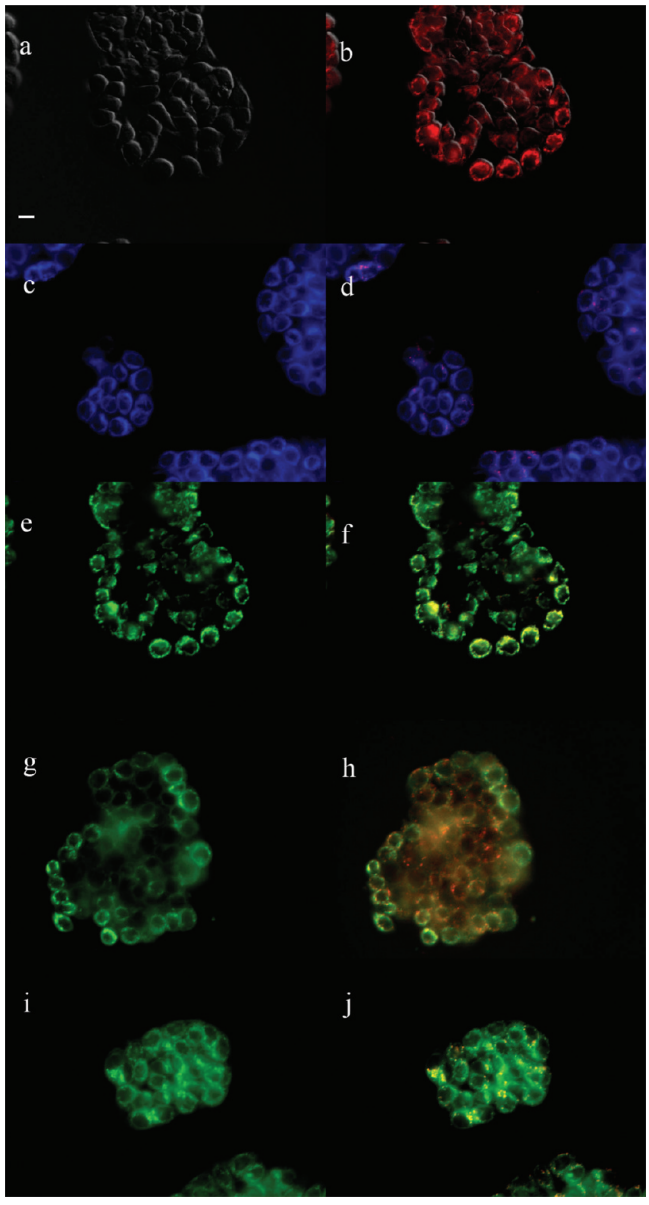

Figure 4. Subcellular fluorescence of *Pc* **5b** in HT-29 cells at 10 μM for 6 h. (a) Phase contrast, (b) overlay of **5b** fluorescence and phase contrast, (c) ER Tracker Blue/White fluorescence, (e) MitoTracker Green fluorescence, (g) BODIPY Ceramide, (i) LysoSensor Green fluorescence, and (d, f, h, j) overlays of organelle tracers with **5b** fluorescence. Scale bar: 10 μm.

compared with **5b**.[53,54] *Pc*–EGFR-L2 conjugates **4b** and **6a** were also found in lysosomes, Golgi, and mitochondria. Lysosomal localization might result from an endocytic pathway of this type of molecule, as we have previously observed.[28,48]

We also investigated potential fluorescence from the *Pc* conjugates on the plasma membrane in order to detect any noninternalized EGFR-bound conjugate. However, no fluorescence was detected by microscopy, indicating that the *Pc* conjugates do not localize on the plasma membrane. In addition, no colocalization was observed with fluorescent probe 1-(4-trimethylammoniumphenyl)-6-phenyl-1,3,5-hexatriene *p*-toluenesulfonate (TMA-DPH) that specifically labels the plasma membrane. This result indicates that the *Pc*–EGFR-L2 conjugates have poor EGFR targeting ability, probably because of their low solubility and high tendency for

dx.doi.org/10.1021/jm201544y | *J. Med. Chem.* 2012, 55, 3725–3738

aggregation. On the other hand, the *Pc*–EGFR-L1 conjugates **5a** and **5b** efficiently target EGFR overexpressing cells and are internalized to a level that is dependent on the degree of EGFR expression.

4. Mouse Studies. *Pc*–peptide conjugate **5b** was chosen for further evaluation in mouse studies due to its low cytotoxicity and rapid accumulation within cells in vitro. Following iv administration of 10 mg/kg of *Pc* **5b**, nude mice showed the emergence of tumor-selective fluorescence indicating that the conjugate was taken up into both A431 and HT-29 subcutaneous tumors. Fluorescence signal which exceeded the background of adjacent skin regions became apparent at 24 h in both tumor types (representative mice shown in Figure 5).

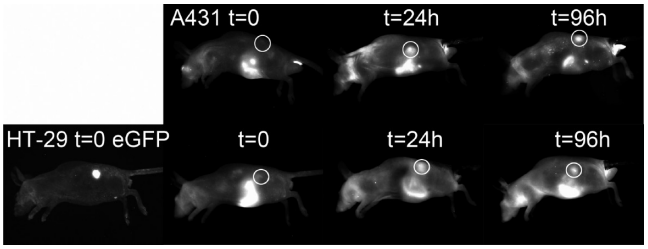

Figure 5. Fluorescent images (exc 630 nm/em 700 nm) of nude mice bearing sc tumor implants of A431 (top) or HT-29 (bottom) cancer cells at various times following iv administration of *Pc* **5b**. The tumor positions are circled, and the left panel of HT-29 mouse shows the eGFP tumor fluorescence (exc 490 nm/em 535 nm).

Microscopically, **5b** deposition in the tumor tissue was not homogeneous but rather seemed to occur in a multifocal pattern, perhaps reflecting regions of greater vascularity (Figure 6); however, sufficient *Pc* **5b** accumulated within the entire tumor to result in a near-IR fluorescence signal distinguishing tumor above adjacent normal tissue. Quantitatively, the signal in the HT-29 tumors declined from 24 to 96 h and could not be readily differentiated from adjacent regions without tumor at 96 h. Preliminary studies with the Kodak In Vivo FX imager, demonstrated that in order to visualize a fluorescence signal, that signal needed to be at least 1.2-fold greater than adjacent regions of the mouse. The fluorescence signal emission in the A431 tumor continued to increase to 96 h (Figure 7), suggesting continued uptake of the *Pc* conjugate over a longer time period in cells overexpressing EGFR.

For purposes of comparison, the two tumor groups were not significantly different in tumor size (A431 = 133.3 ± 28.7 cm^3 and HT-29 = 141.9 ± 21.4 cm^3 at 96 h). Neither tumor demonstrated autofluorescence at the 630/700 nm spectral window at time 0 when compared with adjacent skin surfaces.

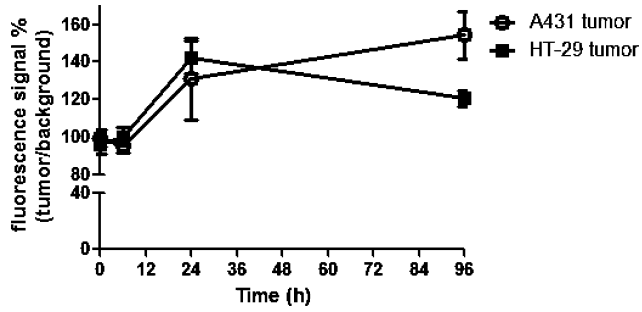

Figure 7. Emission signal of *Pc* **5b** at 700 nm in the sc human tumor xenographs, over the adjacent (background) skin regions, expressed as a percent. To visually distinguish tumors by fluorescence, the tumor needs to be at least 120% of adjacent regions.

In vivo, tumor-associated fluorescence excitable at 630 and emitted at 700 nm was detectable at 24 h. Correspondence of these wavelengths to the *Pc* conjugate spectra indicates uptake of the conjugate by the two subcutaneous human tumor xenografts. While both HT-29 and A431 cells overexpress EGFR, there is a vast difference in the degree of receptor expression, with A431 ~200 times higher EGFR expression than HT-29.[43−45] If the *Pc* conjugate homed to the tumor tissue based solely on the presence of the EGFR ligand, we would not have expected to observe the comparable levels of fluorescence from both tumors at 24 h. Therefore, in addition to tumor attraction based on EGFR–peptide binding, our results suggest significant tumor homing by the *Pc* macrocycle itself, in agreement with the in vitro results (see Figure 2b) and previous observations.[8] The extended fluorescence time within the A431 tumor over the HT-29 tumor suggests that with greater quantities of EGFR comes longer retention and/or greater capacity for selective uptake or reuptake. At times prior to 24 h, we found no or weak signal, suggesting a prolonged time period of plasma circulation with gradual tumor accumulation. A similar pattern of tumor uptake was recently described in a xenograph breast cancer model imaged following administration of a chiral porphyrazine,[55] which showed increasing signal over background up to 48 h post administration. On the other hand, chlorin e6-HSA nanoparticles were recently used for PDT of HT-29 tumor xenograph[56] and shown to have higher tumor-targeting ability and accumulation than free chlorin e_6 as a result of their prolonged blood circulation. Two other chlorin derivatives, HPPH-3Gd(II)ADTPA[57] and TCPCSO3H,[58] were recently shown to accumulate within tumor-bearing mice, reaching maximum accumulation levels at 24 h postadministration.

We detected no signal in adjacent nontumor regions, indicating a high degree of tumor selectivity; however, we

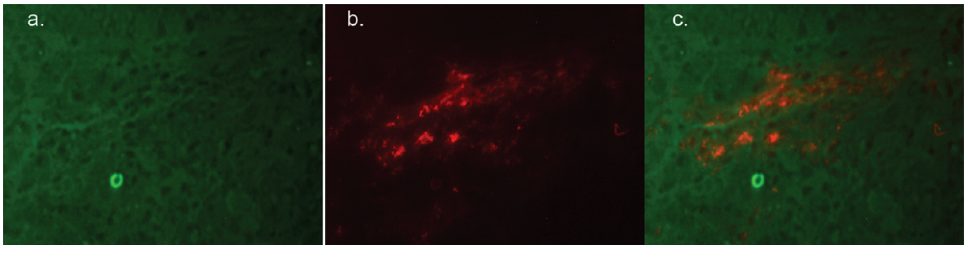

Figure 6. Deposition of *Pc* **5b** in the HT-29 tumor xenograph, 24 h following iv injection. Images show (a) eGFP indicating HT-29 tumor regions, (b) *Pc* **5b** fluorescence, and (c) overlap of tumor and *Pc* deposition.

dx.doi.org/10.1021/jm201544y | *J. Med. Chem.* 2012, 55, 3725−3738

noted that normal gastrointestinal contents in the mice also fluoresced at the near-IR spectra window required for this *Pc*-conjugate. This background fluorescence is difficult to remove in mice because prolonged fasting is not feasible. For imaging of colon or urogenital malignancies, it would likely be necessary to remove fecal material prior to tumor detection.

To evaluate the in vivo stability of conjugate **5b**, the HT-29 tumors were harvested at 24 and 96 h following iv injection and extracted using acetone/methanol mixture. The UV−vis spectra of both the 24 and 96 h tumor extracts in methanol showed the characteristic Q-band absorption of the *Pc* (Supporting Information, Figure S19), indicating that the *Pc* macrocycle has high stability in vivo, allowing for prolonged and selective accumulation within tumor tissue. MALDI-TOF MS indicated that at 24 h, intact conjugate **5b** was still present in the tumor extract, while at 96 h the major *Pc* species detected was *Pc*−PEG-LARL (Supporting Information, Figures S53 and S54). This result suggests that the EGFR-L1 peptide in *Pc* **5b** is slowly degraded within tumor tissue by proteolytic enzymes, mainly losing the two terminal amino acids 96 h after iv injection. This result is in agreement with our previous observations that this type of peptide conjugate can undergo metabolic degradation within tumor cells, with half-life ∼24 h.[59]

CONCLUSIONS

Four *Pc*−peptide conjugates (**4b**, **5a**, **5b**, and **6a**) were designed and synthesized to target EGFR and investigated as potential fluorescence imaging agents for cancers overexpressing EGFR, such as CRC. Two peptide ligands for EGFR containing 6 (LARLLT) and 13 (GYHWYGYTPQNVI) amino acid residues were conjugated to the *Pc* via a short 5-atom or a 13-atom PEG linker. The PEG group enhances the solubility of the *Pc*−peptide conjugates and tends to increase their cellular uptake. Using Autodock, both peptide ligands were found to bind to EGFR, giving low energy (−6 kcal/mol) docking structures, while conjugation to the *Pc* gave even lower docking energies (−8 to −17 kcal/mol) due to additional interactions of the *Pc* macrocycle with hydrophobic residues on EGFR. SPR studies confirmed the binding of *Pc*−peptide conjugates to EGFR.

The short EGFR-L1 peptide conjugates **5a** and **5b** are positively charged and were efficiently internalized by all cell lines (A431, HT-29, HEp2, and Vero cells), localizing preferentially in lysosomes, Golgi, and mitochondria. On the other hand, the 13-residue EGFR-L2 peptide produced highly hydrophobic *Pc* conjugates **4b** and **6a** that, mainly as a result of their poor water solubility and high tendency for aggregation, poorly targeted EGFR at the plasma membranes and were poorly internalized. The amount of *Pc*−EGFR-L1 conjugates, **5a** and **5b**, taken up by cells was dependent on their degree of EGFR expression. While **5a** and **5b**, as well as *Pc*−PEG **3a**, also accumulated within the low EGFR expressing Vero cells, increased uptake was observed with increasing EGFR expression in the human cell lines (A431 > HT-29 > HEp2). The observed uptake into low EGFR expressing cells indicates that the *Pc* macrocycle has a natural tendency to target and accumulate within cancer cells.

All conjugates were found to be nontoxic (IC_{50} > 100 μM) to both low- and overexpressing EGFR cells, with the exception of conjugate **5a** that showed moderate phototoxicity toward A431, HEp2, and Vero cells (IC_{50} = 16, 17, and 47 μM, respectively). None of the conjugates were toxic toward human colorectal HT-29 cells (IC_{50} > 100 μM). This result, in addition to the observed near-IR fluorescence emissions of all *Pc* conjugates at ca. 682 nm with quantum yields in the range 0.10−0.13 and enhanced uptake of **5a** and **5b** by cancer cells, makes these *Pc*−EGFR-L1 conjugates highly promising fluorescent contrast agents for CRC, and potentially other EGFR overexpressing cancers, in particular the least phototoxic (IC_{50} > 100 μM at 1 J/cm^2) β-substituted *Pc*−peptide conjugate **5b**.

Conjugate **5b** was further investigated in nude mice bearing A431 and HT-29 human tumor xenografts. Twenty-four hours after iv administration of **5b**, a clearly near-IR fluorescence signal (exc 630 nm/em 700 nm) was seen over background adjacent tissues in both tumor types. While the fluorescence signal decreased in HT-29 tumors after 24 h, it continued to increase in the A431 tumors up to 96 h, the longest time investigated. The MS analysis of tumor extracts 96 h after iv injection of *Pc*−peptide **5b** indicated partial degradation of the conjugate, by proteolytic enzymes, mainly leading to the cleavage of the last two amino acids of EGFR-L1.

Our studies show that *Pc*−peptide conjugates can be used for near-IR fluorescence imaging of cancers overexpressing EGFR, such as CRC. Because of the hydrophobic nature of the *Pc* macrocycle, a low molecular PEG linker and a polar or charged peptide ligand are required for adequate aqueous solubility and receptor targeting ability. In addition, a β-substituted *Pc* macrocycle appears to be the most suitable for imaging applications due to its lower phototoxicity compared with the corresponding α-substituted macrocycle.

EXPERIMENTAL SECTION

1. Chemistry. All reagents and solvents were purchased from commercial sources and used directly without further purification. Silica gel 60 (230 × 400 mesh) and C18 (200 × 400), both from Sorbent Technologies, were used for column chromatography. Analytical thin-layer chromatography (TLC) was carried out using polyester backed TLC plates 254 (precoated, 200 μm) from Sorbent Technologies. NMR spectra were recorded on AV-400 LIQUID Bruker spectrometer (400 MHz for ^{1}H, 100 MHz for ^{13}C). The chemical shifts are reported in δ ppm using the following deuterated solvents as internal references: acetone-d_6 2.05 ppm (^{1}H), 29.92 ppm (^{13}C); DMF-d_7 8.03 ppm (^{1}H), 163.15 ppm (^{13}C); pyridine-d_5 7.58 ppm (^{1}H), 135.91 ppm (^{13}C). HPLC analyses were carried on a Dionex system equipped with a P680 pump and UVD340U detector. Absorption spectra were measured on a UV−vis NIR scanning spectrometer, using UV-3101PC SHIMADZU (cell positioned) CPS-260 lamp, and emission spectra were obtained on a Fluorolog−HORIBA JOBINVYON (model LFI-3751) spectrofluorimeter. MALDI-TOF mass spectra were recorded on a Bruker ProFlex III mass spectrometer using dithranol as the matrix or Bruker UltrafleXtreme (MALDI-TOF/TOF) using 4-chloro-α-cyanocinnamic acid as the matrix; high resolution ESI mass spectra were obtained on an Agilent Technologies 6210 time-of-flight LC/MS. The melting points (mp) were determined using MEL-TEMP electrothermal instrument. HPLC separation was carried out on a Waters system including a 2545 quaternary gradient module pump, 2489 UV−visible detector, and a fraction collector III. Analytical HPLC was carried out using a XBridge C_{18} 300 Å, 5 μm, 4.6 mm × 250 mm (Waters, USA) column using a stepwise gradient. Semipreparative HPLC was carried out using a XBridge C_{18} 300 Å, 5 μm, 10 mm × 250 mm (Waters, USA) column using a stepwise gradient. The solvent system for peptides consisted of millipure water and HPLC grade acetonitrile, while it consisted of millipure water and HPLC grade methanol for the EGFR-L1 conjugates. *Pc*s **1a**,**b** were synthesized as previously described.[29]

Peptide Synthesis and Conjugations. Applied Biosystems Pioneer peptide synthesis system was used to synthesize peptide sequences. Each peptide was synthesized using Fmoc-PAL-PEG-PS on 0.2 mmol scale using Fmoc strategy of solid-phase peptide synthesis. A 4-fold excess of the L-Fmoc protected amino acids were coupled using HOBt and TBTU as the activating agents. The peptide sequences, prepared

using this methodology, were: LARLLT (EGFR-L1) and GYHWYGYTPQNVI (EGFR-L2). Removal of the Fmoc group from the last amino acid was the final step for each synthesis. This was followed by washing the peptide several times with DMF/dichloromethane and dried under high vacuum for 24 h. The *Pc*−peptide conjugates were synthesized as previously described.[28] In summary, resin containing either GYHWYGYTPQNVI or LARLLT was dissolved in DMF and soaked for 2 h. The *Pc*s were dissolved in DMF and the base and coupling reagents (HOBt and TBTU) added to the *Pc* solutions. The activated mixture was transferred into the reaction vessel containing the resin and left to shake for 4 days. The resin was washed under vacuum several times using DMF, then methanol and finally dichloromethane. A cleavage cocktail consisting of TFA/phenol/TIS/H_2O 88:5:2:5 was added with constant shaking for 4 h. The solution was washed with TFA (2 × 2 mL) into a flask and concentrated under vacuum. Cold diethyl ether was added to the residue and the mixture centrifuged. The *Pc*−EGFR-L1 conjugates were purified using reverse-phase HPLC using a Waters system including a 2545 quaternary gradient module pump, 2489 UV−visible detector, and a fraction collector III. Analytical HPLC was carried out using a XBridge C_{18} 300 Å, 5 μm, 4.6 mm × 250 mm (Waters, USA) column with a stepwise gradient. Semipreparative HPLC was carried out using a XBridge C_{18} 300 Å, 5 μm, 10 mm × 250 mm (Waters, USA) column with a stepwise gradient. The solvent system consisted of Millipure water and HPLC grade methanol (30:70 → 0:100). The purity of the conjugates was >95% as determined by HPLC.

ZnPc ***2a***. A mixture of *Pc* **1a** (80.0 mg, 0.096 mmol) and 1,4-dioxane-2,6-dione (18.0 mg, 0.16 mmol) was dissolved in DMF (1.0 mL) and the solution stirred overnight at room temperature. Water (5.0 mL) was added to the solution to precipitate the product. The solid was filtered under vacuum and washed with water and hexane. The solid was dried under vacuum for 2 days to afford the pure blue solid (80.4 mg, 86.6%), mp 235−236 °C. ^{1}H NMR (pyridine-d_5): δ 10.78−10.71 (s, 1H, −COOH), 10.17−9.41 (m, 7H, Ar−H), 8.44−8.23 (m, 6H, Ar−H), 8.01−7.71 (m, 3H, Ar−H), 6.04 (br, 1H, N−H), 4.55 (d, *J* = 12.4 Hz, 2H, CH_2O), 4.47 (d, *J* = 10.5 Hz, 2H, CH_2O), 1.73−1.59 (m, 27H, $C(CH_3)_3$). ^{13}C NMR (pyridine-d_5): δ 168.3, 168.2, 156.6, 155.9, 155.8, 154.7, 154.3, 154.0, 152.9, 150.6, 150.4, 150.1, 149.8, 142.4, 140.1, 140.0, 137.8, 137.7, 136.2, 136.0, 135.8, 135.5, 134.3, 134.8, 131.54, 128.46, 128.3, 124.8, 124.2, 124.0, 123.7, 123.4, 122.8, 122.5, 121.4, 120.6, 120.5, 120.4, 120.2, 119.4, 118.1, (Ar−C) 73.1, 70.5 (OCH_2), 35.8, 32.4 (Ar−C, $C(CH_3)_3$). MS (MALDI-TOF) *m*/*z* 968.319 $[M + H]^+$, calcd for $C_{54}H_{50}N_9O_5Zn$ 967.323. UV−vis (DMF): λ_{max} (log ε) 346 nm (5.04), 614 nm (4.80), 680 nm (5.50).

ZnPc ***2b***. A mixture of *Pc* **1b** (50.0 mg, 0.06 mmol) and 1,4-dioxane-2,6-dione (11.3 mg, 0.1 mmol) was dissolved in DMF (0.5 mL) and the solution stirred overnight at room temperature. The mixture was purified as **2a** above to afford the pure blue solid (53.5 mg, 92.2%), mp 249−250 °C. ^{1}H NMR (pyridine-d_5): δ 10.84−10.77 (s, 1H, −COOH), 10.01−9.35 (m, 8H, Ar−H), 8.50−8.21 (m, 5H, Ar−H), 8.10−7.90 (m, 1H, Ar−H), 7.54−7.41 (m, 2H, Ar−H), 6.74 (br, 1H, N−H), 4.69 (d, *J* = 5.4 Hz, 2H, CH_2O), 4.60 (d, *J* = 5.6 Hz, 2H, CH_2O), 1.75−1.64 (m, 27H, $C(CH_3)_3$). ^{13}C NMR (pyridine-d_5): δ 173.9, 168.43, 168.38, 160.0, 159.7, 154.8, 154.7, 154.6, 154.5, 154.3, 153.9, 153.8, 153.5, 153.4, 153.0, 150.6, 150.4, 150.1, 140.8, 139.4, 139.2, 137.0, 136.8, 134.2, 134.0, 131.0, 127.7, 124.7, 122.0, 120.8, 120.7, 120.3, 119.8, 112.5, 111.6 (Ar−C) 72.5, 69.9 (OCH_2), 35.8, 31.7 (Ar−C, $C(CH_3)_3$). MS (MALDI-TOF) *m*/*z* 968.314 $[M + H]^+$, calcd for $C_{54}H_{50}N_9O_5Zn$ 968.323. UV−vis (DMF): λ_{max} (log ε) 351 nm (4.86), 611 nm (4.58), 679 nm (5.33).

ZnPc ***3a***. *Pc* **2a** (30.0 mg, 0.032 mmol) was dissolved in DMF (400 μL). Et_3N (4.0 mg, 0.041 mmol), HOBt (4.6 mg, 0.034 mmol), and *tert*-butyl-12-amino-4,7,10-trioxadodecanoate (10.8 mg, 0.039 mmol) were added to the reaction mixture. EDCI (5.3 mg, 0.034 mmol) was then added in one portion. The reaction solution was stirred for 3 days at room temperature, diluted using ethyl acetate (10 mL), and washed subsequently with water (20 mL × 2). The organic layer was dried over anhydrous sodium sulfate. The solvent was evaporated and the crude product purified on silica column eluted with mixed solvents of DCM/methanol (98:2→ 96:4) to afford a blue solid (30.0 mg, 76.5%). ^{1}H NMR (DMF-d_7): δ 9.60−9.01 (m, 7H, Ar−H), 8.45−8.15 (m, 5H, Ar−H), 8.00−7.77 (m, 3H, Ar−H), 7.63−7.49 (m, 2H, Ar−H), 4.27−4.15 (m, 4H, CH_2O), 3.62−3.57 (m, 3H, CH_2O), 3.54−3.47 (m, 9H, CH_2O), 3.42−3.37 (m, 2H, CH_2O), 2.44−2.39 (m, 2H, CH_2CO), 1.82−1.78 (m, 27H, $C(CH_3)_3$), 1.40 (s, 9H, $C(CH_3)_3$). ^{13}C NMR (DMF-d_7): δ 171.7, 170.5, 168.8, 168.7, 156.8, 156.2, 155.6, 155.5, 155.2, 155.1, 155.0, 154.7, 154.6, 154.4, 154.3, 154.20, 154.16, 154.0, 153.4, 153.3, 153.2, 152.4, 152.1, 152.04, 151.96, 142.3, 140.03, 139.98, 139.9, 139.6, 137.64, 137.57, 137.5, 137.2, 135.10, 135.06, 143.5, 131.7, 131.6, 130.1, 129.4, 128.7, 128.6, 128.4, 123.6, 123.5, 123.3, 122.6, 122.4, 122.3, 122.0, 120.3, 120.1, 120.0, 119.8, 119.6, 119.0, 118.9, 117.5 (Ar−C), 80.8 ($O-C(CH_3)_3$), 72.4, 72.1, 71.20, 71.18, 71.15, 71.1, 71.0, 70.5, 70.32, 70.30, 67.2 (OCH_2), 39.64, 39.61, ($COCH_2$), 32.7, 32.6 (Ar−C, $C(CH_3)_3$), 28.5 ($N-C(CH_3)_3$). MS (MALDI-TOF) *m*/*z* 1170.497 $[M - {}^tBu + H]^+$, calcd for $C_{63}H_{66}N_{10}O_9Zn$ 1170.431. The protected *Pc* conjugate was dissolved in a mixture of DCM/TFA (4 mL/4 mL) and stirred at 0 °C for 3 h. The solvent was evaporated, the residue treated with 2N NaOH (2 mL) and then extracted by ethyl acetate (15 mL). The product was dried under vacuum to afford blue product (24.0 mg, 89.3%), mp 191−192 °C. ^{1}H NMR (DMF-d_7): δ 10.15−10.13 (s, 1H, −COOH), 9.59−9.08 (m, 7H, Ar−H), 8.42−8.10 (m, 5H, Ar−H), 7.95−7.82 (m, 3H, Ar−H), 7.61−7.52 (m, 2H, Ar−H), 4.25−4.11 (m, 4H, CH_2O), 3.79−3.57 (m, 12H, CH_2O), 3.41−3.37 (m, 2H, CH_2O), 2.51−2.48 (m, 2H, CH_2CO), 1.79 (s, 27H, $C(CH_3)_3$). ^{13}C NMR (pyridine-d_5): δ 173.7, 170.5, 168.7, 156.9, 156.2, 155.4, 154.5, 153.7, 152.6, 145.6, 142.6, 140.2, 139.8, 137.6, 135.2, 134.6, 131.7, 128.7, 123.5, 122.7, 122.4, 120.0, 119.1, 117.7 (Ar−C), 72.5, 72.2, 71.3, 70.4, 67.8 (OCH_2), 35.5 ($COCH_2$), 32.6 (Ar−C, $C(CH_3)_3$). MS (MALDI-TOF) *m*/*z* 1170.485 $[M]^+$, calcd for $C_{63}H_{66}N_{10}O_9Zn$ 1170.431. UV−vis (DMF): λ_{max} (log ε) 349 nm (4.90), 612 nm (4.61), 678 nm (5.35).

ZnPc ***3b***. *Pc* **2b** (30.0 mg, 0.032 mmol) was dissolved in DMF (400 μL). Et_3N (4.0 mg, 0.041 mmol), HOBt (4.6 mg, 0.034 mmol), and *tert*-butyl-12-amino-4,7,10-trioxadodecanoate (10.8 mg, 0.039 mmol) were added to the reaction solution, and the solution was stirred for 20 min. EDCI (5.3 mg, 0.034 mmol) was added to the reaction solution in one portion. The reaction was then treated as **3a** above to afford a blue solid (32.2 mg, 82.3%). ^{1}H NMR (acetone-d_6): δ 9.87−9.77 (m, 1H, Ar−H), 9.07−7.40 (m, 16H, Ar−H), 3.99 (s, 2H, CH_2O), 3.87 (s, 2H, CH_2O), 3.58−3.54 (m, 2H, CH_2O), 3.45 (s, 8H, CH_2O), 3.38 (s, 2H, CH_2O), 3.22 (s, 2H, CH_2O), 2.36−2.33 (m, 2H, CH_2CO), 1.88−1.78 (m, 27H, $C(CH_3)_3$), 1.37 (s, 9H, $C(CH_3)_3$). ^{13}C NMR (DMF-d_7): δ 171.8, 170.7, 169.3, 169.2, 162.4, 160.8, 160.4, 155.0, 154.8, 154.3, 154.2, 141.4, 140.0, 139.8, 137.6, 136.7, 136.4, 134.5, 128.6, 125.2, 123.4, 123.0, 121.4, 121.3, 120.9, 120.0, 112.8, 111.7 (Ar−C), 81.0 ($O-C(CH_3)_3$), 72.6, 72.4, 71.5, 71.43, 71.36, 71.3, 70.6, 67.8 (OCH_2), 32.8 (Ar−C, $C(CH_3)_3$), 28.7 ($N-C(CH_3)_3$). MS (MALDI-TOF) *m*/*z* 1227.682 $[M + H]^+$, 1170.495 $[M - {}^tBu + H]^+$, calcd for $C_{67}H_{75}N_{10}O_9Zn$ 1227.501, $C_{63}H_{66}N_{10}O_9Zn$ 1170.431. The protected *Pc* conjugate was then deprotected as **3a** above to afford a blue solid (25.3 mg, 88.3%), mp 161−163 °C. ^{1}H NMR (DMF-d_7): δ 10.42−10.33 (s, 1H, COOH), 9.57−9.32 (m, 6H, Ar−H), 9.09−8.75 (m, 1H, Ar−H), 8.55−8.20 (m, 4H, Ar−H), 8.15−8.00 (m, 2H, Ar−H), 7.99−7.81 (m, 1H, Ar−H), 7.65−7.50 (m, 2H, Ar−H), 4.36 (d, *J* = 7.2 Hz, 2H, CH_2O), 4.28 (d, *J* = 5.1 Hz, 2H, CH_2O), 3.65−3.57 (m, 12H, CH_2O), 3.41−3.37 (m, 2H, CH_2O), 2.55−2.48 (m, 2H, CH_2O), 1.85−1.74 (m, 27H, $C(CH_3)_3$). ^{13}C NMR (DMF-d_7): δ 173.7, 170.6, 169.2, 169.1, 160.64, 160.58, 160.25, 160.18, 155.3, 155.22, 155.16, 155.1, 155.0, 154.9, 154.8, 154.7, 154.3, 154.2, 1154.15, 154.11, 153.0, 153.9, 153.4, 153.3, 153.2, 153.1, 141.5, 141.4, 140.1, 140.0, 139.8, 137.7, 137.64, 137.55, 137.5, 136.5, 136.2, 134.8, 134.7, 134.6, 128.3, 128.2, 126.2, 125.0, 123.3, 123.2, 122.8, 122.0, 121.2, 121.11, 121.06, 120.8, 120.7, 119.9, 119.8, 112.7, 111.6, (Ar−C), 72.4, 72.1, 71.28, 71.25, 71.14, 71.10, 70.4, 68.3, 67.7 (OCH_2), 39.7, 36.8 ($COCH_2$), 32.6 (Ar−C, $C(CH_3)_3$). MS (MALDI-TOF) *m*/*z* 1170.508 $[M]^+$, calcd for $C_{63}H_{66}N_{10}O_9Zn$ 1170.431. UV−vis (DMF): λ_{max} (log ε) 350 nm (4.65), 610 nm (4.41), 676 nm (5.19).

ZnPc Conjugate ***4b***. Resin (60.0 mg) containing 0.0052 mmol GYHWYGYTPQNVI was transferred into a reaction vial. DMF was added (5:1, DMF/resin) and soaked for 2 h. The resin was washed four times with DMF. *Pc* **2b** (10.0 mg, 0.010315 mmol) was weighed into a vial and DMF (200 μL) added. Then HOBt (1.4 mg, 0.010315 mmol), TBTU (3.3 mg, 0.010315 mmol), and DIEA (5.39 μL, 0.030946 mmol) were added to the *Pc* solution. The mixture was stirred for 30 min, transferred into the vial containing the resin, and left to shake for 3 days. The resin was washed under vacuum using DMF (until DMF was clear), followed by methanol and finally DCM. A cleavage cocktail, TFA/phenol/TIS/H_2O (88:5:2:5), was added and shaken constantly for 4 h. The solution was then washed with TFA (2 × 2 mL) into a 50 mL flask under vacuum. Cold diethylether was added to the residue and the mixture centrifuged. The precipitate was then sonicated in water and centrifuged several times to give the title compound (9.2 mg, 35.0%), mp 211−212 °C. ^{1}H NMR (DMF-d_7): δ 9.51−9.20 (m, 5H, Ar−H), 8.45−8.10 (m, 9H, Ar−H), 7.80−7.75 (m, 2H, Ar−H), 7.70−7.50 (m, 2H, Ar−H), 7.35−7.20 (m, 24H, Ar−H), 7.07−6.91 (m, 14H, Ar−H), 6.80−6.70 (m, 4H, Ar−H), 6.65−6.53 (m, 9H, Ar−H), 4.68−4.30 (m, 12H, CH_2NH), 4.24−3.65 (m, 4H, CH_2O/CH_2NH), 3.45−3.30 (m, 4H, CH_2O/CH_2NH), 2.25−2.04 (m, 2H, CH_2CO), 2.01−1.75 (m, 21H, $C(CH_3)_3/CH_2$), 1.33 (s, 5H, CH_3), 1.26 (s, 2H, CH_2), 1.18−1.10 (m, 4H, CH_2), 1.00−0.94 (m, 8H, CH_2), 0.85−0.75 (m, 18H, CH_3). MS (MALDI-TOF) *m/z* 2545.04 $[M]^+$, calcd for $C_{131}H_{148}N_{28}O_{23}Zn$ 2545.0563. UV−vis (DMF): λ_{max} (log ε) 351 nm (4.44), 610 nm (4.07), 677 nm (4.87).

ZnPc Conjugate ***5a***. Resin (25.7 mg, 0.0052 mmol) containing LARLLT was transferred into a reaction vial. DMF was added (5:1, DMF/resin) and left to soak for 4 h, after which it was washed four times with DMF. *Pc* **3a** (10.0 mg, 0.010315 mmol) was weighed into a 2.0 mL vial and DMF (200 μL) added. DIEA (6.4 μL, 0.036745 mmol) was added to the solution and stirred for 1 h. Then HOBt (1.8 mg, 0.013321 mmol) and HATU (4.0 mg, 0.010521 mmol) were added to the *Pc* solution. The mixture was added to the resin and left to shake for 4 days and cleaved as described above for *Pc* **4b.** The product was purified using reverse-phase HPLC eluted by water/methanol (30:70 → 0:100) to afford a blue solid (7.6 mg, 79.2%), mp 151−152 °C. ^{1}H NMR (DMF-d_7): δ 10.18, 10.13 (s, 1H, N−H), 9.67−9.20 (m, 5H, Ar−H), 8.55−8.45 (m, 3H, Ar−H), 8.25−8.15 (m, 2H, Ar−H), 8.13−8.05 (m, 1H, Ar−H), 7.97−7.86 (m, 5H, Ar−H), 7.85−7.79 (m, 2H, Ar−H), 7.61−7.47 (m, 5H, Ar−H), 7.20 (s, 1H, Ar−H), 7.13 (s, 1H, Ar−H), 4.39−4.01 (m, 26H, CH_2O/CH_2NH), 3.77−3.70 (m, 3H, CH_2O), 3.56−3.50 (m, 12H, CH_2O), 3.43−3.31 (m, 3H, CH_2O), 2.55−2.41 (m, 2H, CH_2CO), 2.01−1.92 (m, 3H, CH_2), 1.85−1.71 (m, 27H, $C(CH_3)_3$/7H, CH_2), 1.69−1.62 (m, 3H, CH_2), 1.43−1.35 (m, 4H, CH_2), 1.21−1.15 (m, 4H, CH_2), 0.94−0.87 (m, 20H, CH_3). ^{13}C NMR (DMF-d_7): δ 175.5, 175.3, 174.10, 174.07, 173.7, 173.4, 170.5, 168.8, 168.7, 160.3, 159.9, 158.7, 156.8, 156.2, 155.6, 155.3, 155.1, 154.4, 152.4, 152.1, 140.0, 137.9, 137.6, 135.1, 134.5, 131.7, 128.6, 123.4, 122.6, 122.4, 120.0, 119.0, 117.5, 116.1 (Ar−C), 72.3, 72.0, 71.3, 71.2, 71.0, 70.9, 70.3, 68.2, 68.0, 66.3 (OCH_2), 60.1, 55.2, 54.6, 54.0, 53.5. 51.8, 41.9, 41.3, 41.2, 39.5, 37.2 (CH_2) 32.6 (Ar−C, $C(CH_3)_3$), 29.4, 26.5, 25.6, 25.5, 24.0, 23.8, 23.5, 22.3, 22.0, 21.8, 20.7, 17.5 (CH_3). MS (MALDI-TOF) *m/z* 1837.907 $[M + H]^+$, calcd for $C_{94}H_{125}N_{20}O_{15}Zn$ 1837.892. MS-MS (MALDI-TOF-TOF) *m/z* 1839.90 [PcPEG−LARLLT + H]$^+$, 1822.88 [PcPEG−LARLLT-NH_2 + H]$^+$, 1794.88 [PcPEG−LARLLT-$CONH_2$ + H]$^+$, 1723.042 [PcPEG−LARLL-NH_2 + H]$^+$, 1580.75 [PcPEG−LARL-CO + H]$^+$, 1339.56 [PcPEG−LA-NH_2 + H]$^+$, 1268.52 [PcPEG−L-NH_2 + H]$^+$, 1240.53 [PcPEG−L-CO + H]$^+$, 1155.44 [PcPEG−NH_2 + H]$^+$, calcd for $C_{94}H_{125}N_{20}O_{15}Zn$ 1837.892, $C_{94}H_{124}N_{19}O_{15}Zn$ 1822.882, $C_{93}H_{124}N_{19}O_{14}Zn$ 1794.887, $C_{90}H_{117}N_{18}O_{13}Zn$ 1721.834, $C_{83}H_{106}N_{17}O_{11}Zn$ 1580.755, $C_{72}H_{83}N_{12}O_{10}Zn$ 1339.565, $C_{69}H_{78}N_{11}O_9Zn$ 1268.528, $C_{68}H_{78}N_{11}O_8Zn$ 1240.533, $C_{63}H_{67}N_{10}O_8Zn$ 1155.444. UV−vis (DMF): λ_{max} (log ε) 348 nm (4.79), 612 nm (4.56), 680 nm (5.33).

ZnPc Conjugate ***5b***. Resin (25.7 mg, 0.0052 mmol) containing LARLLT was transferred into a reaction vial. DMF was added (5:1, DMF/resin) and left to soak for 4 h, after which it was washed four times with DMF. *Pc* **3b** (10.0 mg, 0.010315 mmol) was weighed into a 2.0 mL vial and DMF (200 μL) added. DIEA (6.4 μL, 0.036745 mmol) was added to the solution and stirred for 1 h. Then HOBt (1.8 mg, 0.013321 mmol) and HATU (4.0 mg, 0.010521 mmol) were added to the *Pc* solution. The mixture was added to the resin and left to shake for 4 days. It was then cleaved and purified using reverse-phase HPLC eluted by water/methanol (30:70 → 0:100) to afford a blue solid (8.1 mg, 84.4%, mp 167−168 °C). ^{1}H NMR (DMF-d_7): δ 10.40, 10.35 (s, 1H, N−H), 9.67−9.20 (m, 5H, Ar−H), 8.57−8.45 (m, 3H, Ar−H), 8.30−8.25 (m, 2H, Ar−H), 8.13−8.05 (m, 2H, Ar−H), 7.97−7.86 (m, 3H, Ar−H), 7.85−7.79 (m, 2H, Ar−H), 7.61−7.47 (m, 5H, Ar−H), 7.18 (s, 1H, Ar−H), 7.12 (s, 1H, Ar−H), 4.37 (d, *J* = 7.6, 4H, CH_2O), 4.29−4.21 (m, 9H, CH_2NH), 3.77−3.70 (m, 16H, CH_2NH), 3.65−3.57 (m, 12H, CH_2O), 3.54−3.43 (m, 2H, CH_2NH), 3.37−3.29 (m, 3H, CH_2NH), 2.61−2.56 (m, 2H, CH_2CO), 2.01−1.92 (m, 2H, CH_2), 1.91−1.71 (m, 27H, $C(CH_3)_3$/7H, CH_2), 1.69−1.58 (m, 5H, CH_2), 1.39−1.36 (m, 4H, CH_2), 1.17−1.15 (m, 4H, CH_2), 0.95−0.86 (m, 20H, CH_3). ^{13}C NMR (DMF-d_7): δ 175.5, 175.3, 174.1, 174.0, 173.7, 173.6, 173.4, 170.6, 169.2, 169.1, 160.2, 159.9, 158.8, 154.6, 154.2, 153.7, 140.2, 139.8, 136.7, 136.3, 128.6, 128.4, 122.8, 122.2, 121.4, 120.9, 119.3, 116.3 (Ar−C), 72.4, 72.2, 71.3, 71.1, 71.0, 70.4, 68.2, 68.1, 66.3 (OCH_2), 60.1, 55.2, 54.6, 54.0, 53.5. 51.8, 41.9, 41.34, 41.29, 39.7, 37.2 (CH_2) 32.6 (Ar−C, $C(CH_3)_3$), 29.4, 26.5, 25.7, 25.6, 25.5, 24.0, 23.8, 23.5, 22.4, 22.0, 21.8, 20.7, 17.6 (CH_3). MS (MALDI-TOF) *m/z* 1837.925 $[M + H]^+$, calcd for $C_{94}H_{125}N_{20}O_{15}Zn$ 1837.892. MS-MS (MALDI-TOF-TOF) *m/z* 1839.90 [PcPEG−LARLLT + H]$^+$, 1822.88 [PcPEG−LARLLT-NH_2 + H]$^+$, 1794.88 [PcPEG−LARLLT-$CONH_2$ + H]$^+$, 1721.83 [PcPEG−LARLL-NH_2 + H]$^+$, 1580.75 [PcPEG−LARL-CO + H]$^+$, 1339.56 [PcPEG−LA-NH_2 + H]$^+$, 1268.52 [PcPEG−L-NH_2 + H]$^+$, 1240.53 [PcPEG−L-CO + H]$^+$, 1155.44 [PcPEG−NH_2 + H]$^+$, calcd for $C_{94}H_{125}N_{20}O_{15}Zn$ 1837.892, $C_{94}H_{124}N_{19}O_{15}Zn$ 1822.882, $C_{93}H_{124}N_{19}O_{14}Zn$ 1794.887, $C_{90}H_{117}N_{18}O_{13}Zn$ 1721.834, $C_{83}H_{106}N_{17}O_{11}Zn$ 1580.755, $C_{72}H_{83}N_{12}O_{10}Zn$ 1339.565, $C_{69}H_{78}N_{11}O_9Zn$ 1268.528, $C_{68}H_{78}N_{11}O_8Zn$ 1240.533, $C_{63}H_{67}N_{10}O_8Zn$ 1155.444. UV−vis (DMF): λ_{max} (log ε) 352 nm (4.79), 610 nm (4.52), 677 nm (5.29).

ZnPc Conjugate ***6a***. Resin (60.0 mg, 0.0052 mmol) containing GYHWYGYTPQNVI was transferred into a reaction vial. DMF was added (5:1, DMF/resin) and left to soak for one hour, after which it was washed four times with DMF. *Pc* **3a** (12.1 mg, 0.010315 mmol) was weighed into a 2.0 mL vial and DMF (200 μL) added. Then HOBt (1.4 mg, 0.010315 mmol), HATU (3.9 mg, 0.010315 mmol), and DIEA (5.39 μL, 0.030946 mmol) were added to the *Pc* solution. The mixture was stirred for 5 min, transferred into the reaction chamber containing the resin, and left to shake for 3 days. Cleavage from solid support and purification proceeded as described above for *Pc* **4b** to afford a blue solid (11.5 mg, 40.5%, mp 208−209 °C). ^{1}H NMR (DMF-d_7): δ 10.40, 10.35 (s, 1H, N−H), 9.51−9.20 (m, 6H, Ar−H), 8.45−8.10 (m, 10H, Ar−H), 7.80−7.75 (m, 2H, Ar−H), 7.70−7.50 (m, 2H, Ar−H), 7.45−7.20 (m, 30H, Ar−H), 7.15−6.95 (m, 14H, Ar−H), 6.90−6.78 (m, 4H, Ar−H), 6.74−6.65 (m, 9H, Ar−H), 4.75−4.10 (m, 16H, CH_2O/CH_2NH), 4.04−3.65 (m, 7H, CH_2O/CH_2NH), 2.25−2.04 (m, 6H, CH_2CO), 2.01−1.75 (m, 21H, $C(CH_3)_3/CH_2$), 1.43 (s, 4H,, CH_2), 1.31 (s, 3H, CH_2), 1.21−1.15 (m, 4H, CH_2), 1.05−1.00 (m, 8H, CH_2), 0.94−0.85 (m, 19H, CH_3). MS (MALDI-TOF) *m/z* 2748.17 $[M]^+$, calcd for $C_{140}H_{165}N_{29}O_{27}Zn$ 2748.1723. MS-MS (MALDI-TOF-TOF) *m/z* 2751.19 [PcPEG−GYHWYGYTPQNVI]$^+$, 2733.25 [PcPEG−GYHWYGYTPQNVI-NH_2]$^+$, 2702.25 [*Pc*-PEG−GYHWYGYTPQNVI-$CONH_2$]$^+$, 2165.86 [PcPEG−YHWYGYT-NH_2-OH]$^+$, 1670.78 [PcPEG−GYHW-$CONH_2$]$^+$, 1490.70. [PcPEG−GYH-$CONH_2$]$^+$, 1346.53 [*Pc*-PEG−GY-$CONH_2$]$^+$, 1226.34 [PcPEG−G]$^+$, 1155.44 [PcPEG−NH_2 + H]$^+$, calcd for $C_{140}H_{165}N_{29}O_{27}Zn$ 2748.17, $C_{140}H_{164}N_{28}O_{27}Zn$ 2733.16, $C_{139}H_{164}N_{28}O_{26}Zn$ 2705.17, $C_{115}H_{123}N_{21}O_{19}Zn$ 2165.86, $C_{90}H_{95}N_{17}O_{12}Zn$ 1669.66, $C_{79}H_{85}N_{15}O_{11}Zn$ 1483.58, $C_{73}H_{78}N_{12}O_{10}Zn$ 1346.53, $C_{65}H_{70}N_{12}O_9Zn$ 1226.47, $C_{63}H_{67}N_{10}O_8Zn$ 1155.44. UV−vis (DMF): λ_{max} (log ε) 345 nm (3.84), 612 nm (4.25), 680 nm (4.60).

2. Spectroscopic Studies. All absorption spectra were measured on UV−vis NIR scanning spectrometer UV-3101PC SHIMADZU

(cell positioned) equipped with a CPS-260 lamp. The DMF solvent used was HPLC grade, and it was the solvent of choice because it dissolved all the Pcs relatively good. Stock solutions (1000 μM, 1.0 mL) of all *Pcs* were prepared and the dilutions were prepared by spiking 20−80 μL of the corresponding stock solution into 10.0 mL of solvent. Emission spectra were obtained on a Fluorolog−HORIBA JOBINVYON (model LFI-3751) spectrofluorimeter. The optical densities of the solutions used for emission studies ranged between 0.04 and 0.05 at excitation wavelengths. All experiments were carried out within 4 h of solution preparation at room temperature (23−25 °C) with 10 mm path length spectrophotometric cell. The fluorescent quantum yields (Φ_f) were determined using a secondary standard method.[30] By comparison with ZnPc (Φ_f = 0.17) as a reference, the values of fluorescence were obtained in DMF solvent.[31]

3. Computational and SPR Studies. Docking of EGFR-L1, L2 peptides and their conjugates to EGFR protein extracellular domain was performed using AUTODOCK 4 software.[32,33] EGFR crystal structure was obtained from a Protein Data Bank (PDB code: 1nql).[34] Solvent molecules were removed from the pdb file. Polar hydrogen atoms were added to the structure. Three dimensional structures of peptides and their conjugates, EGFR-L1, EGFR-L2, **4b**, **5b**, and **6a** were generated using InsightII (Accelrys Inc., Sandiego, CA). Structures were subjected to 300 K and molecular dynamics (MD) followed by simulated annealing MD.[35] The final structure from simulated MD was energy minimized and used for docking studies. A grid box with dimensions of 128 × 128 × 128 Å^3 was used for calculations. For EGFR-L1 peptide and **5b** docking, a grid box was created with amino acid residue on EGFR Asn134 as center of the grid box, and for EGFR-L2, **4b**, and **6a** docking, a grid box was created near the EGF binding site on EGFR.[26,27] For **4b**, **5b**, and **6a**, the zinc atom was included in addition to the atom types of the peptide/protein for grid calculations. In all these ligand molecules, rotatable bonds were allowed to rotate during docking calculations. For docking, 50 runs with 10 million energy evaluations were carried out using Lamarkian genetic algorithm. Docking calculations were performed on Linux cluster on high performance supercomputers at LSU Baton Rouge. Docked structures were listed in increasing order of energy, and low-energy clusters were used as the most probable binding models. The energy reported is for the lowest energy docked structure from a cluster of conformations. Structures from low-energy docking were displayed and analyzed using PyMol software.

The surface plasmon resonance (SPR) experiments were performed using Biacore X100 (GE Health Sciences) at 25 °C.[36,37] Immobilization of EGFR (obtained from Leinco Technologies, St. Louis, MO) was performed by standard amine coupling procedure on a CM5 chip. The carboxyl groups on the sensor chip were activated by a solution containing 0.2 M *N*-ethyl-*N*-(dimethylaminopropyl) carbodiimide and 0.05 M *N*-hydroxysuccinimide (35 μL solution, flow rate 5 μL/min). Running buffer consisted of 0.01 M HEPES, 0.15 M NaCl, 3 mM EDTA, 0.005% Tween at pH 7.5. Regeneration buffers were 50% acid cocktail and glycine 100 mM at pH 2.5. The EGF ligand was obtained from Abcam, Inc. (Cambridge, MA).

4. Cell Studies. All tissue culture medium and reagents were purchased from Invitrogen (Carlsbad, CA). Human carcinoma HEp2 cells, human epidermoid carcinoma A431, human colorectal adenocarcinoma HT-29, and *Cercopithecus aethiops* kidney Vero cells were purchased from ATCC. HT-29 cells were cultured and maintained in McCoy's 5a Medium Modified supplemented with 10% FBS and 1% antibiotic (penicillin−streptomycin). HT-29 cells were infected with a lentivirus containing the enhanced green fluorescent protein (eGFP; virus purchased from Biogenova, Ellicott City, MD). Green fluorescent cells were sorted by flow cytometery and expanded to generate a line termed "HT-29 eGFP". Both A431 and Vero cells were cultured and maintained in ATCC formulated DMEM supplemented with 10% FBS and 1% antibiotic (penicillin−streptomycin). HEp2 cells were cultured and maintained in 50:50 ATCC formulated DMEM/Advanced MEM containing 10% FBS and 1% antibiotic (penicillin−streptomycin). The cells were split twice weekly to maintain a subconfluent stock. All compound solutions were filter-sterilized using a 0.22 μm syringe filter. A 32 mM stock solution was prepared for each *Pc* by dissolving in DMSO containing 5% Cremophor EL (as a nonionic emulsifier) to avoid compound precipitation upon dilution into media. From this solution, a 400 μM stock was also prepared in desired medium and filter-sterilized using a 0.22 μm syringe filter.

4.1. Time-Dependent Cellular Uptake. HEp2 cells and A431 cells were plated at 7500 per well in a Costar 96-well plate and allowed to grow for 48 h. Vero cells were plated at 7500 per well in a Costar 96-well plate and allowed to grow for 24 h. HT-29 cells were plated at 7500 per well in a Costar 96-well plate and allowed to grow for 96 h. *Pc* stock solutions (32 mM) were diluted to 10 μM *Pc* solutions in media and added to the cells at different time periods of 0, 1, 2, 4, 8, and 24 h. Uptake of the compounds was stopped by removing loading medium and washing once with PBS. Cells were solubilized by adding 0.25% Triton X-100 in PBS. The *Pc* concentration was determined by reading its fluorescence emission at 650/700 nm (excitation/emission) using a BMG FLUOstar plate reader (Cary, NC). Cell number was quantified using CyQuant reagent.

4.2. Dark Cytotoxicity. The cells were plated and allowed to grow as described above. *Pc* stock solutions (32 mM) were diluted to concentrations of 25, 50, 100, and 125 μM in medium and added to cells for 24 h. The loading medium was removed, and medium containing Cell Titer Blue was added to determine the toxicity of the compounds (viable cells were measured fluorescently at 570/615 nm); untreated cells were considered 100% viable and cells treated with 0.2% saponin as 0% viable.

4.3. Phototoxicity. The cells were plated and allowed to grow as described above. *Pc* stock solutions (32 mM) were diluted to concentrations of 6.25, 12.5, 25, 50, and 100 μM in medium and added to cells for 24 h. The loading medium was removed, and fresh medium was added. The conjugates were exposed to light for 20 min using a light system (Newport) for a light dose of ∼1 J/cm^2. The plates were chilled at 5 °C using a cooling block. Water was used as a filter for IR radiation. The plates were then incubated for another 24 h, followed by removing medium and adding medium containing Cell Titer Blue to determine the toxicity of the compounds.

4.4. Microscopy. The cells were inoculated in a glass-bottom 6-well plate (MatTek) and allowed to grow for 48 h. The cells were then exposed to 10 μM for each *Pc* for 6 h. Organelle tracers were obtained from Invitrogen and used at the following concentrations: LysoSensor Green 50 nM, MitoTracker Green 250 nM, ER Tracker Blue/White 100 nM, and BODIPY FL C5 Ceramide 1 μM. Images were acquired using a Leica DMRXA microscope with 40× NA 0.8dip objective lens and DAPI, GFP, and Texas Red filter cubes (Chroma Technologies).

5. In Vivo Uptake Studies. For the animal studies, Nu/nu mice were purchased from Charles Rivers Laboratories at 6 weeks of age. After approximately 2 weeks of quarantine, mice were implanted with tumor cells subcutaneously in the upper flank. For these injections, each cell line was cultured to approximately 75% confluence, then dissociated with trypsin, and concentrated by centrifugation. Because the two tumor lines were found to grow at different rates in nude mice, 1 × 10^6 A431 cells and 2 × 10^6 HT-29 eGFP cells were implanted in a volume of 100 μL. The injection material consisted of 4 parts DMEM and 1 part MatriGel basement membrane matrix (BD biosciences). Tumors were allowed to develop until palpable (approximately 6 days for A431 cells and 9 days for HT-29 eGFP cells), after which mice were imaged for time = 0, then injected through the tail vein with 20 μL of a 10 mM solution of *Pc* **5b** in 10% DMSO and 5% Cremophor EL in PBS, for a dose of ∼10 mg/kg. The mice were then observed for acute adverse responses to the injected *Pc* and returned to their box until imaged. Prior to imaging at selected time points after *Pc* administration, mice were anesthetized with isoflurane gas to effect then imaged individually for 30 s at excitation 630 nm and emission 700 nm (x630/m700) in a Kodak In Vivo FX whole animal imager. All animal experiments were conducted by adherence to a protocol approved by the LSU IACUC committee.

To rule out toxicity related to the concentration of DMSO (10%) and Cremophor EL (5%) used to solubilize the conjugates, an additional viability assay was performed in vitro to estimate cancer tissue exposure in vivo (see Supporting Information for details).

Addition of DMSO and Cremophor EL to culture media at either blood volume or extracellular fluid volume dilutions showed no effect on cell viability over a 96 h period, suggesting it is unlikely that these agents resulted in toxicity in vivo after dilution and distribution.

To quantify relative fluorescence within the image of the tumor region, a region-of-interest (roi) was drawn around the tumor and the mean pixel intensity (mpi) of this roi was divided by the mpi's of three adjacent skin areas to obtain a percent of tumor fluorescence over adjacent regions. To visually distinguish one roi as more fluorescent than adjacent skin, we found that the roi needed to be at least 120%.

At 24 and 96 h following iv injection of *Pc* **5b**, the HT-29 tumor tissue was harvested from mice and flash frozen. The tissue was kept in 5 mL of acetone/methanol (5:1) at −20 °C overnight, then crushed repeatedly using a mortar, filtered, and the organic solvents removed under reduced pressure. The residues were analyzed by MS-MALDI-TOF and UV−vis spectrophotometry. Frozen sections of tumor were cut to 10 μm thickness and mounted on glass slides. Tissues were immediately imaged for both eGFP indicating regions of HT-29 tumor and near-IR indicating *Pc* fluorescence using Chroma 41017 (450−490 nm excitation, 500−550 nm emission) and Omega Optical 140-2 (570−645 nm excitation, 668−723 nm emission) filter sets, respectively.

■ ASSOCIATED CONTENT

Ⓢ Supporting Information

NMR spectra, MS, HPLC chromatograms, phototoxicity and dark toxicity plots, subcellular localization microscopy. This material is available free of charge via the Internet at http://pubs.acs.org.

■ AUTHOR INFORMATION

Corresponding Author

*Phone: 225-578-7405. Fax: 225-578-3458. E-mail: vicente@lsu.edu.

Notes

The authors declare no competing financial interest.

■ ACKNOWLEDGMENTS

This work was supported by the National Institutes of Health, grant number R21 CA139385. Partial support from R25 GM069743 is also acknowledged. Satyanarayana-Jois was supported by grants from the National Center for Research Resources (5P20RR016456-11) and the National Institute of General Medical Sciences (8 P20GM103424-11) from the National Institutes of Health via the Louisiana Biomedical Research Network (LBRN). Computational docking studies were conducted via the Louisiana Optical Network Initiative (LONI). We thank Dr. Balamurugan Subramanian for assistance with the SPR experiments.

■ ABBREVIATIONS USED

Pc, phthalocyanine; CRC, colorectal cancer; CLE, confocal laser endomicroscopy; EGFR, epidermal growth factor receptor; PDT, photodynamic therapy; DMF, dimethylformamide; DMSO, dimethylsulfoxide; THF, tetrahydrofuran; DBN, 1,5-diazabicyclo(4.3.0)non-5-ene; DMAE, dimethylaminoethanol; TFA, trifluoroacetic acid; DIEA, *N*,*N*-diisopropylethylamine; TBTU, 2-(1*H*-benzotriazol-1-yl)-1,1,3,3-tetramethyluronium tetrafluoroborate; HATU, 2-(1*H*-azabenzotriazol-1-yl)-1,1,3,3-tetramethyluronium hexafluorophosphate; EDCI, 1-ethyl-3-(3-dimethylaminopropyl)-carbodiimide hydrochloride; TEA, triethylamine; Fmoc, fluorenylmethyloxycarbonyl; TIS, triisopropylsilane; HOBt, 1-hydroxybenzotriazole; PBS, phosphate buffered saline; FBS, fetal bovine serum; DMEM, Dulbecco's Modified Eagle's Medium; ER, endoplasmic reticulum

■ REFERENCES

(1) Colon and Rectum Cancer What Are the Key Statistics for Colorectal Cancer? *American Cancer Society Detailed Guide*; American Cancer Society: Atlanta, 2011; www.cancer.org/Cancer/ColonandRectumCancer/DetailedGuide/colorectal-cancer-key-statistics.

(2) Kiesslich, R.; Goetz, M.; Vieth, M.; Galle, P. R.; Neurath, M. F. Technology insight: confocal laser endoscopy for in vivo diagnosis of colorectal cancer. *Nature Clin. Pract. Oncol.* **2007**, *4*, 480−490.

(3) Van den Broek, F. J.; Fockens, P.; Dekker, F. New developments in colonic imaging. *Aliment. Pharmacol. Ther.* **2007**, *26*, 91−99.

(4) Kantsevoy, S. V.; Adler, D. G.; Conway, J. D.; Diehl, D. L.; Farraye, F. A.; Kaul, V.; Kethu, S. R.; Kwon, R. S.; Mamula, P.; Rodriguez, S. A.; Tierney, W. M.; Comm, A. T. Confocal laser endomicroscopy. *Gastrointest. Endoscopy* **2009**, *70* (2), 197−200.

(5) Leznoff, C. C.; Lever, A. B. P. In *Phthalocyanines: Properties and Applications*; VCH: Weinheim, 1989−1996; Vols. *1*−*4*.

(6) Sharman, W. M.; Van Lier, J. E. Synthesis of phthalocyanines. In *The Porphyrin Handbook*; Kadish, K. M., Smith, K. M., Guilard, R., Eds.; Academic Press: Boston, 2003, Vol. *15*, pp 1−60.

(7) Liu, T. M.; Chu, S. W.; Sun, C. K.; Lin, B. L.; Cheng, P. C.; Johnson, I. Multiphoton confocal microscopy using a femtosecond Cr:forsterite laser. *Scanning* **2001**, *23*, 249−254.

(8) Ben-Hur, E.; Chan, W.-S. Phthalocyanines in photobiology and their medical applications. In *The Porphyrin Handbook*; Kadish, K. M., Smith, K. M., Guilard, R., Eds.; Academic Press: Boston, 2003; Vol. *19*, pp 1−35.

(9) Erk, P.; Hengelsberg, H. Phthalocyanines dyes and pigments. In *The Porphyrin Handbook*; Kadish, K. M., Smith, K. M., Guilard, R., Eds.; Academic Press: Boston, 2003; Vol. *19*, pp 106−146.

(10) Kimura, M.; Shirai, H. Enzyme-like catalytic reactions of metallophthalocyanines and polymeric metallophthalocyanines. In *The Porphyrin Handbook*; Kadish, K. M., Smith, K. M., Guilard, R., Eds.; Academic Press: Boston, 2003; Vol. *19*, pp 151−173.

(11) Dougherty, T. J.; Gomer, C. J.; Henderson, B. W.; Jori, G.; Kessel, D.; Korbelik, M.; Moan, J.; Peng, Q. Photodynamic therapy. *J. Natl. Cancer Inst.* **1998**, *90*, 889−905.

(12) Pandey, R. K. Recent advances in photodynamic therapy. *J. Porphyrins Phthalocyanines* **2000**, *4*, 368−373.

(13) Sharman, W. M.; van Lier, J. E.; Allen, C. M. Targeted photodynamic therapy via receptor mediated delivery systems. *Adv. Drug Delivery Rev.* **2004**, *56*, 53−76.

(14) Savellano, M. D.; Hasan, T. Photochemical targeting of epidermal growth factor receptor: a mechanistic study. *Clin. Cancer Res.* **2005**, *11*, 1658−1668.

(15) Hudson, R.; Boyle, R. W. Strategies for selective delivery of photodynamic sensitizers to biological targets. *J. Porphyrins Phthalocyanines* **2004**, *8*, 954−975.

(16) Pérez-Soler, R. HER1/EGFR Targeting: refining the strategy. *Oncologist* **2004**, *9*, 58−67.

(17) Meric-Bernstam, F.; Hung, M.-C. Advances in targeting human epidermal growth factor receptor-2 signaling for cancer therapy. *Clin. Cancer Res.* **2006**, *12*, 6326−6330.

(18) Spano, J.−P.; Lagorce, C.; Atlan, D.; Milano, G.; Domont, J.; Bnamouzig, R.; Attar, A.; Benichou, J.; Martin, A.; Morere, J. −F.; Raphael, M.; Penault-Llorca, F.; Breau, J.−L.; Fagard, R.; Khayat, D.; Wind, P. Impact of EGFR expression on colorectal cancer patient prognosis and survival. *Ann. Oncol.* **2005**, *16*, 102−108.

(19) Galizia, G.; Iieto, E.; Ferraraccio, F.; De Vita, F.; Castellano, P.; Orditura, M.; Imperatore, V.; La Mura, A.; La Manna, G.; Pinto, M.; Catalano, G.; Pignatelli, C.; Ciardiello, F. Prognostic significance of epidermal growth factor receptor expression in colon cancer patients undergoing curative surgery. *Ann. Surg. Oncol.* **2006**, *13*, 823−835.

(20) Dougherty, U.; Sehdev, A.; Cerda, S.; Mustafi, R.; Little, N.; Yuan, W.; Jagadeeswaran, S.; Chumsangsri, A.; Delgado, J.; Tretiakova, M.; Joseph, L.; Hart, J.; Cohen, E. E.; Aluri, L.; Fichera, A.;

Bissonnette, M. Epidermal growth factor receptor controls flat dysplastic aberrant crypt foci development and colon cancer progression in the rat azoxymethane model. *Clin. Cancer Res.* **2008**, *14*, 2253−2262.
(21) Loeffler-Ragg, J.; Schwentner, I.; Sprinzl, G. M.; Zwierzina, H. EGFR inhibition as a therapy for head and neck squamous cell carcinoma. *Expert Opin. Invest. Drugs* **2008**, *17*, 1517−1531.
(22) Molema, G. Design of vascular endothelium-specific drug-targeting strategies for the treatment of cancer. *Acta Biochim. Pol.* **2005**, *52*, 301−310.
(23) Dane, K. Y.; Chan, L. A.; Rice, J. J.; Daugherty, P. S. Isolation of cell specific peptide ligands using fluorescent bacterial display libraries. *J. Immunol. Methods* **2006**, *309*, 120−129.
(24) Frochot, C.; Stasio, B. D.; Vanderesse, R.; Belgy, M.-J.; Dodeller, M.; Guillemin, F.; Viriot, M.-L.; Barberi-Heyob, M. Interest of RGD-containing linear or cyclic peptide targeted tetraphenylchlorin as novel photosensitizers for selective photodynamic therapy. *Bioorg. Chem.* **2007**, *35*, 205−220.
(25) Song, S. X.; Liu, D.; Peng, J. L.; Sun, Y.; Li, Z. H.; Gu, J. R.; Xu, Y. H. Peptide ligand-mediated liposome distribution and targeting to EGFR expressing tumor in vivo. *Int. J. Pharm.* **2008**, *363*, 155−161.
(26) Song, S.; Liu, D.; Peng, J.; Deng, H.; Guo, Y.; Xu, L. X.; Miller, A. D.; Xu, Y. Novel peptide ligand directs liposomes toward EGFR high-expressing cancer cells in vitro and in vivo. *FASEB J.* **2009**, *23*, 1396−1404.
(27) Li, Z.; Zhao, R.; Wu, X.; Sun, Y.; Yao, M.; Li, J.; Xu, Y.; Gu, J. Identification and characterization of a novel peptide ligand of epidermal growth factor receptor for targeted delivery of therapeutics. *FASEB J.* **2005**, *19*, 1978−1985.
(28) Sibrian-Vazquez, M.; Ortiz, J.; Nesterova, I. V.; Fernández-Lázaro, F.; Sastre-Santos, A.; Soper, S. A.; Vicente, M. G. H. Synthesis and properties of cell-targeted Zn(II)−phthalocyanine−peptide conjugates. *Bioconjugate Chem.* **2007**, *18*, 410−420.
(29) Ongarora, B. G.; Hu, X.; Li, H.; Fronczek, F. R.; Vicente, M. G. H. Syntheses and properties of trimethylaminophenoxy-substituted Zn(II)-phthalocyanines. *Med. Chem. Commun.* **2012**, *3*, 179−194.
(30) Brykina, G. D.; Uvarova, M. I.; Koval, Y. N.; Shpigun, O. A. High-performance liquid chromatography of metal tetra-4-*tert*-butylphthalocyanines. *J. Anal. Chem.* **2001**, *56*, 940−944.
(31) Zorlu, Y.; Dumoulin, F.; Durmus, M.; Ahsen, V. Comparative studies of photophysical and photochemical properties of solketal substituted platinum(II) and zinc(II) phthalocyanine sets. *Tetrahedron* **2010**, *66*, 3248−3258.
(32) Morris, G. M.; Goodsell, D. S.; Halliday, R. S.; Huey, R.; Hart, W. E.; Belew, R. K.; Olson, A. J. Automated docking using a Lamarckian genetic algorithm and empirical binding free energy function. *J. Comput. Chem.* **1998**, *19*, 1639−1662.
(33) Huey, R.; Morris, G. A.; Olson, A. J.; Goodsell, D. S. A semiempirical free energy force field with charge-based desolvation. *J. Comput. Chem.* **2006**, *28*, 1145−1152.
(34) Ferguson, K. M.; Berger, M. B.; Mendrola, J. M.; Cho, H.; Leahy, D. J.; Lemmon, M. A. EGF activates its receptor by removing interactions that autoinhibit ectodomain dimerization. *Mol. Cell* **2003**, *11*, 507−517.
(35) Sutcliffe, M. J. Structure determination from NMR data II. Computational approaches. In *NMR of Macromolecules: A Practical Approach*; Roberts, G. C. K., Ed.; Oxford University Press: New York, 1993; pp 359−390.
(36) Komolov, K. E.; Koch, K. W. Application of surface plasmon resonance spectroscopy to study G-protein coupled receptor signaling in surface plasmon resonance. *Methods Mol. Biol.* De Moi, N. J. Fischer, M. J. E., Eds.; Springer Science: New York; 2010; Chapter 17.
(37) Berezov, A.; Zhang, H.-T.; Greene, M. I.; Murali, R. Disabling ErbB receptors with rationally designed exocyclic mimetics of antibodies: structure−function analysis. *J. Med. Chem.* **2001**, *44*, 2565−2574.
(38) Sibrian-Vazquez, M.; Jensen, T. J.; Hammer, R. P.; Vicente, M. G. H. Peptide-mediated cell transport of water soluble porphyrin conjugates. *J. Med. Chem.* **2006**, *49*, 1364−1372.
(39) Sibrian-Vazquez, M.; Jensen, T. J.; Vicente, M. G. H. Influence of the number and distribution of NLS peptides on the photosensitizing activity of multimeric porphyrin−NLS. *Org. Biomol. Chem.* **2010**, *8*, 1160−1172.
(40) Rocha-Lima, C. M.; Soares, P. H.; Raez, L. E.; Singal, R. EGFR targeting of solid tumors. *Cancer Control* **2007**, *14* (3), 295−304.
(41) Gulli, L. F.; Palmer, K. C.; Chen, Y. Q.; Reddy, K. B. Epidermal growth factor-induced apoptosis in A431 cells can be reversed by reducing the tyrosine kinase activity. *Cell Growth Differ.* **1996**, *7* (2), 173−178.
(42) Kawamoto, T.; Sato, J. D.; Le, A.; Polikoff, J.; Sato, G. H.; Mendelsohn, J. Growth-stimulation of A431 cells by epidermal growth-factor—identification of high-affinity receptors for epidermal growth-factor by an anti-receptor monoclonal antibody. *Proc. Natl. Acad. Sci. U.S.A.* **1983**, *80* (5), 1337−1341.
(43) Haigler, H.; Ash, J. F.; Singer, S. J.; Cohen, S. Visualization by fluorescence of the binding and internalization of epidermal growth factor in human carcinoma cells A-431. *Proc. Natl. Acad. Sci. U.S.A.* **1978**, *75* (7), 3317−3321.
(44) Macfarla, D.; Sommervi, Rg. Vero cells (*Cercopithecus aethiops* kidney)—growth characteristics and viral susceptibility for use in diagnostic virology. *Archiv. Ges. Virusforsch* **1969**, *27* (2−4), 379−385.
(45) Pellegrini, R.; Centis, F.; Martignone, S.; Mastroianni, A.; Tagliabue, E.; Tosi, E.; Menard, S.; Colnaghi, M. I. Characterization of a monoclonal-antibody directed against the epidermal growth-factor receptor-binding site. *Cancer Immunol. Immunother.* **1991**, *34* (1), 37−42.
(46) Magné, N.; Fischel, J. L.; Dubreuil, A.; Formento, P.; Poupon, M.-F.; Laurent-Puig, P.; Milano, G. Influence of epidermal growth factor receptor (EGFR), p53 and intrinsic MAP kinase pathway status of tumour cells on the antiproliferative effect of ZD1839 ("Iressa"). *Br. J. Cancer* **2002**, *86*, 1518−1523.
(47) Giannopoulou, E.; Antonacopoulou, A.; Matsouka, P.; Kalofonos, H. P. Autophagy: novel action of Panitumumab in colon cancer. *Anticancer Res.* **2009**, *29* (12), 5077−5082.
(48) Sibrian-Vazquez, M.; Jensen, T. J.; Fronczek, F. R.; Hammer, R. P.; Vicente, M. G. H. Synthesis and characterization of positively charged porphyrin−peptide conjugates. *Bioconjugate Chem.* **2005**, *16* (4), 852−863.
(49) Futaki, S.; Suzuki, T.; Ohashi, W.; Yagami, T.; Tanaka, S.; Ueda, K.; Sugiura, Y. Arginine-rich peptides. An abundant source of membrane-permeable peptides having potential as carriers for intracellular protein delivery. *J. Biol. Chem.* **2001**, *276*, 5836−5840.
(50) Zuhorn, I. S.; Hoekstra, D. On the mechanism of cationic amphiphile-mediated transfection. To fuse or not to fuse: is that the question? *J. Membr. Biol.* **2002**, *189* (3), 167−179.
(51) Rothbard, J. B.; Jessop, T. C.; Lewis, R. S.; Murray, B. A.; Wender, P. A. Role of membrane potential and hydrogen bonding in the mechanism of translocation of guanidinium-rich peptides into cells. *J. Am. Chem. Soc.* **2004**, *126*, 9506−9507.
(52) He, J.; Haney, R. M.; Vora, M.; Verkhusha, V. V.; Stahelin, R. V.; Kutateladze, T. G. Molecular mechanism of membrane targeting by the GRP1 PH domain. *J. Lipid Res.* **2008**, *49* (8), 1807−1815.
(53) Rao, R. V.; Hermel, E.; Castro-Obregon, S.; del Rio, G.; Ellerby, L. M.; Ellerby, H. M.; Bredesen, D. E. Coupling endoplasmic reticulum stress to the cell death program. Mechanism of caspase activation. *J. Biol. Chem.* **2001**, *276*, 33869−33874.
(54) Kessel, D. Correlation between subcellular localization and photodynamic efficacy. *J. Porphyrins Phthalocyanines* **2004**, *8*, 1009−1014.
(55) Trivedi, E. R.; Harney, A. S.; Olive, M. B.; Podgorski, I.; Moin, K.; Sloane, B. F.; Barrett, A. G. M.; Meade, T. J.; Hoffman, B. M. Chiral porphyrazine near-IR optical imaging agent exhibiting preferential tumor accumulation. *Proc. Natl. Acad. Sci. U.S.A.* **2010**, *107* (4), 1284−1288.
(56) Jeong, H.; Huh, M.; Lee, S. J.; Koo, H.; Kwon, I. C.; Jeong, S. Y.; Kim, K. Photosensitizer-conjugated human serum albumin nanoparticles for effective photodynamic therapy. *Theranostics* **2011**, *1*, 230−239.

(57) Spernyak, J. A.; White, W. H., III; Ethirajan, M.; Patel, N. J.; Goswami, L.; Chen, Y.; Turowski, S.; Missert, J. R.; Batt, C.; Mazurchuk, R.; Pandey, R. K. Hexylether derivative of pyropheophorbide-a (HPPH) on conjugating with 3 gadolinium(III) aminobenzyldiethylenetriaminepentaacetic acid shows potential for in vivo tumor imaging (MR, fluorescence) and photodynamic therapy. *Bioconjugate Chem.* **2010**, *21*, 828−835.
(58) Dabrowski, J. M.; Krzykawska, M.; Arnaut, L. G.; Pereira, M. M.; Monteiro, C. J. P.; Simoes, S.; Urbanska, K.; Stochel, G. Tissue uptake study and photodynamic therapy of melanoma-bearing mice with a nontoxic, effective chlorin. *ChemMedChem.* **2011**, *6* (9), 1715−1726.
(59) Sibrian-Vazquez, M.; Jensen, T. J.; Vicente, M. G. H. Synthesis, characterization, and metabolic stability of porphyrin−peptide conjugates bearing bifunctional signaling sequences. *J. Med. Chem.* **2008**, *51*, 2915−2923.